

---

# A DIFFERENTIABLE MODEL OF NUCLEIC ACID DYNAMICS

---

**Ryan K. Krueger**

School of Engineering and Applied Sciences  
Harvard University  
Cambridge, MA  
ryan\_krueger@g.harvard.edu

**Megan C. Engel**

Department of Biological Sciences  
University of Calgary  
Calgary, AB, Canada  
megan.engel@ucalgary.ca

**Ryan Hausen**

Institute for Data Intensive Engineering and Science  
Johns Hopkins University  
Baltimore, MD  
rhausen@jhu.edu

**Michael P. Brenner**

School of Engineering and Applied Sciences  
Harvard University  
Cambridge, MA  
Department of Physics  
Harvard University  
Cambridge, MA  
brenner@seas.harvard.edu

## ABSTRACT

Developing physics-based models for molecular simulation requires fitting many unknown parameters to experimental datasets of diverse properties. Fitting such diverse data is typically carried out piecemeal, resulting in a “zoo” of disconnected but highly related models. Here, we leverage recently developed methods for computing low-variance gradient estimates with automatic differentiation to facilitate the extensible, reproducible, and transparent fitting of the physics-based DNA model oxDNA. We demonstrate simultaneous fitting to structural, mechanical, and thermodynamic data using a variety of techniques, including enhanced sampling, external forcing, cluster-move Monte Carlo schemes, and micro- and millisecond timescales, and fit oxDNA to a range of target properties, such as twist-stretch couplings and duplex melting temperatures. We also demonstrate how gradients can serve as an efficient means of sensitivity analysis through which we uncover the surprising importance of the cross-stacking interaction in oxDNA. Though grounded in oxDNA, this work provides a framework for extensible, community-driven force field development more generally that will yield rapidly improved models and subsequent physical insights for systems ranging from RNA to protein to their interactions with inorganic materials.

## 1 Introduction

Physics-based molecular simulations using coarse-grained potentials are a cornerstone of *in silico* biophysical modeling. When sufficiently accurate, they provide a unique way to study a biophysical system beyond available experimental data [1]. Such models have provided deep insights ranging from viral assembly [2, 3, 4, 5] to protein folding [6, 7, 8] to chromosomal organization [9, 10]. Recent successes in experimental nucleic acid nanotechnology [11, 12, 13] combined with the comparative simplicity of DNA and RNA relative to proteins renders DNA/RNA modeling an attractive and active area of research.

Yet, while recent years have seen extraordinary progress in the accuracy of large scale machine learning (ML) models, from large language models [14, 15] to protein structure prediction [16], the accuracy of coarse-grained potentials has stagnated. The machine learning examples clearly demonstrate that increased model accuracy unlocks enormous value. Recently, Donoho hypothesized [17] that *frictionless reproducibility*, the ease of reproducing and iteratively improving models, is the major factor leading to dramatic ML model improvement. Within ML, model parameters are almost universally fit via gradient-based optimization, datasets are clearly partitioned into train, validation, and test subsets, objective functions are clearly-defined, and trained models and fitting procedures are often publicly available

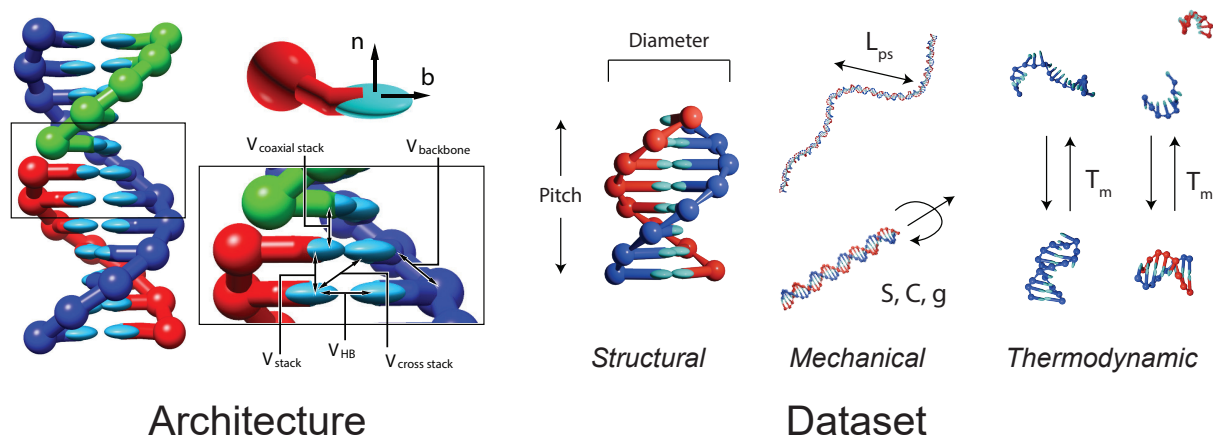


Figure 1: The formulation of force field parameter fitting as an optimization problem akin to neural network training. The choice of functional form is analogous to fixing a neural network *architecture*, where geometric parameters control the relative positions of beads in a rigid body and Hamiltonian parameters describe the interactions between these beads. The objective function is formulated as a function of ground truth *data*, typically derived from experiment, and is evaluated by means of forward simulations. The oxDNA model was originally fit to three classes of experimental data: structural (e.g. helical pitch and diameter), mechanical (e.g. persistence length  $L_{ps}$ ), and thermodynamic (e.g. melting temperatures  $T_m$ ). The depiction of the oxDNA architecture is adapted from Ref. [39].

via popular open-source tools such as GitHub and Hugging Face. These standardized and transparent fitting procedures enable rapid technological innovation.

Here, we demonstrate how this paradigm can be applied to fitting coarse-grained, physics-based potentials. We apply *differentiable programming*, the backbone of machine learning algorithms whereby gradients are computed via automatic differentiation (AD), to an exemplar of coarse-grained molecular modeling: nucleic acid force field development.

Despite resounding successes for particular coarse-grained DNA and RNA models [18, 19, 20, 21, 22, 23], both types of force field development are plagued by suboptimal parameter fitting methods that are often opaque and hard to reproduce. Force field parameters are typically the result of heroic fitting procedures with significant hand-design [24, 18, 25, 26, 27, 28, 29, 30]. Even force fields that have been fit through comparatively more principled approaches such as Iterative Boltzmann Inversion [31, 24], maximum likelihood methods [32], or Newton Inversion [33] often use piecemeal approaches to parameter optimization: each type of interaction (e.g. hydrogen bonding, excluded volume, stacking, etc) is treated individually – often with differing parameterization schemes – without simultaneous optimization of all parameter types. As such, existing models cannot be easily adapted to model new effects (e.g. non-canonical base-pairing, electrostatics) or new experimental data. Often, entirely new models are invented to treat experimental inconsistencies without knowing whether this is truly required given the initial model parameterization.

A case in point is the recent MADna model of Assenza and Pérez [24], developed to model mechanical properties that are poorly captured by existing models (e.g. oxDNA, 3SPN). Rather than fine-tuning an existing, otherwise successful DNA model, Assenza and Pérez were required to develop an entirely new model. Indeed, expanded parameterizations of DNA/RNA models often appear years after the original model release [34, 35, 36, 37, 38], attesting to the difficulty and laboriousness of refining models where parameterization is nontransparent and unsystematic. The ultimate result is a fragmented “zoo” of models that each require months or years of trial-and-error parameter fitting despite attempting to represent similar datasets.

Here, we focus on solving these issues within oxDNA, a coarse-grained model with a physics-based and interpretable potential energy function. The model has enjoyed extensive validation against experiment [40] and is therefore widely employed in the DNA nanotechnology community for both (i) deriving *in silico* biophysical insights in systems such as nanotweezers and gels [41, 42, 43], and (ii) complementing experimental studies in subjects ranging from strand displacement [44, 45] to DNA origami [46, 47]. By focusing on an experimentally-relevant model with a relatively complex and expressive energy function, we are forced to confront the three main issues of traditional differentiable MD. First, computing the gradient through long unrolled simulations imposes a significant memory overhead as well

as numerical instabilities [48, 49]. Second, many fundamental algorithms in molecular simulation are not end-to-end differentiable (e.g. cluster-move Monte Carlo schemes). Third, decades of research have been dedicated to optimizing MD algorithms to increase the accessible timescales, but many of these optimizations are lost upon reimplementation in an automatic differentiation framework.

We surmount these technical challenges using a novel method for stochastic gradient estimation [50, 51], making it possible to use gradient-descent to fit force field parameters to the three classes of experimental data to which oxDNA was originally fit: structural, mechanical, and thermodynamic. Each class of data poses a unique set of challenges that are not present in toy models previously studied with differentiable MD. For example, calculation of mechanical properties, such as persistence length or stretch modulus, typically requires micro- and millisecond-scale simulations to sample many uncorrelated states, line-fitting procedures to infer summary statistics, and the application of external forces and torques. Similarly, melting temperature calculations require particularly complex simulations, involving enhanced sampling, cluster-move Monte Carlo algorithms, and temperature extrapolation. Our approach allows us to combine the methods developed for each individual class of data to fit parameters to *single* objective functions that jointly target structural, mechanical, and thermodynamic properties, allowing for the first time a systematic, simultaneous parameter optimization for different loss functions and for different interaction terms in the potential energy function. We also demonstrate how the calculated gradients can be adapted for sensitivity analyses, enabling the rapid derivation of physical insights. Our results not only agree with existing literature, but also reveal new insights. As an example, we find cross-stacking interaction parameters are much more influential than naively expected.

We hope that this work serves as a launching point for what we believe will be paradigm shift in extensible, collaborative, community-driven force field development. We make all code for the parameter optimizations presented in this work available at the following GitHub repository: <https://github.com/rkruegs123/jax-dna>.

## 2 Results

### 2.1 Differentiable Force Field Implementation

To carry out gradient-descent on the parameters of oxDNA, we first implemented the oxDNA energy function in JAX, a state-of-the-art AD library for scientific computing [52]. There are several versions of oxDNA as additional features such as sequence-specificity and major-minor grooving have been added since the parameterization of the original model. While we implement all versions of oxDNA in our framework, here (unless otherwise stated) we focus our results on the sequence-averaged version of oxDNA2, the latest version of oxDNA. To simulate systems of DNA with our implementation, we use JAX-MD, an end-to-end differentiable molecular dynamics engine written in JAX [53]. We benchmark our implementation against the standalone oxDNA code [54, 55], involving both highly-optimized C++ and CUDA implementations, and find that our implementation is 2-3x slower (Figure S1).

Despite this performance cost, the JAX implementation offers two key advantages. First, since we write our energy function in an AD framework, forces are computed automatically from energy functions. This significantly reduces the barrier to experimenting with modified functional forms of the energy function, and also permits the application of arbitrary (continuous and differentiable) external forces and torques. Second, since the code can be compiled to a range of hardware accelerators, we can immediately run simulations on GPU and TPU without reimplementing the force field in a separate framework. Therefore, our JAX implementation can be seen as complementary to the existing standalone and LAMMPS [56] implementations of oxDNA: beyond permitting gradient-based optimization, it enables flexibility and extensibility for force field development.

We now in turn consider each of the three classes (i.e. structural, mechanical, and thermodynamic) of data used to fit force field parameterizations in oxDNA.

### 2.2 Structural Optimization

Structural properties are the most amenable to optimization via differentiable MD, since the simulations required to compute such properties are shortest in time and smallest in system size. As a first step, we fit a subset of oxDNA parameters to target pitch and propeller twist values. We sought to evaluate whether the pathwise estimator (Figure 2A), whereby gradients are computed directly through an unrolled numerical simulation, is sufficient for optimizing oxDNA parameters for structural properties. We find that the pathwise estimator has numerous numerical and computational limitations; the backwards calculation imposes significant time and memory overhead, and yields gradients whose magnitude increases sharply with simulation time (Figure 2B-D). The gradients calculated through short simulations for computing structural properties were too numerically unstable for optimization (Figure S2A). At the same time, we also evaluated the score function estimator for structural optimization, in which batches of simulations are performed and

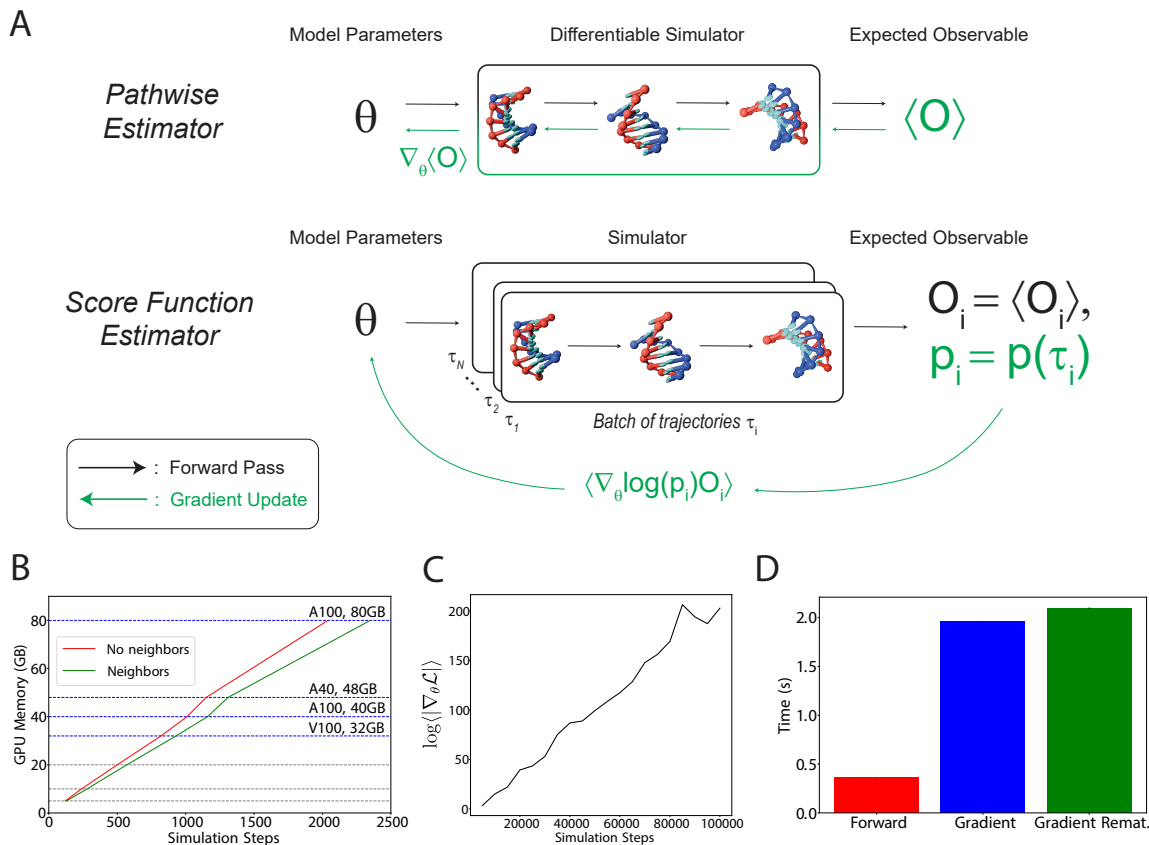


Figure 2: Traditional differentiable molecular dynamics does not scale to oxDNA, a representative experimentally-relevant force field. **A**. The traditional methods for stochastic gradient estimation in which gradients are directly calculated via a differentiable simulator (i.e. the pathwise estimator) or the gradients of (log) probabilities of individual trajectories are scaled by a reward defined for each trajectory (i.e. the score function estimator). Conventional differentiable molecular dynamics relies on the pathwise estimator (see Supporting Information for an evaluation of the score function estimator). **B**. The memory cost per pathwise estimator calculation as a function of simulation length for a 60 bp duplex, the prototypical system for evaluating structural properties, revealing the maximum simulation length ( $\sim 2500$  steps) feasible on currently available hardware. **C**. The (log) average absolute value of the gradient of the RMSE of the measured pitch vs. the target pitch as a function of simulation length for simulations of a 60 bp duplex. Gradient rematerialization (also called gradient *checkpointing*) was used to permit gradient calculations at longer simulation lengths at the cost of runtime (see Supporting Information). **D**. A comparison of the time to simulate an eight base pair duplex for 2000 timesteps with and without gradient calculation.

the probability of such simulations are increased or decreased according to the calculated observable (Figure 2A). This method also did not yield sufficient signal for optimization (Figure S2B).

As such, we turned to a recently developed method of stochastic gradient estimation that directly operates at the level of unnormalized steady state probability distributions (Figure 3A). This method was first introduced as a general method for differentiable Monte Carlo in the context of variational quantum Monte Carlo by Zhang et al. [50] and machine-learned potentials for molecular simulation [51], where it was termed DiffTRE, serving as a low-variance score function estimator that effectively computes the objective function as an integral over unnormalized probability distributions; see *Materials and Methods* for details. This estimator circumvents the memory and numerical issues associated with traditional differentiable MD by only differentiating the energy of reference states sampled from a set of simulations.



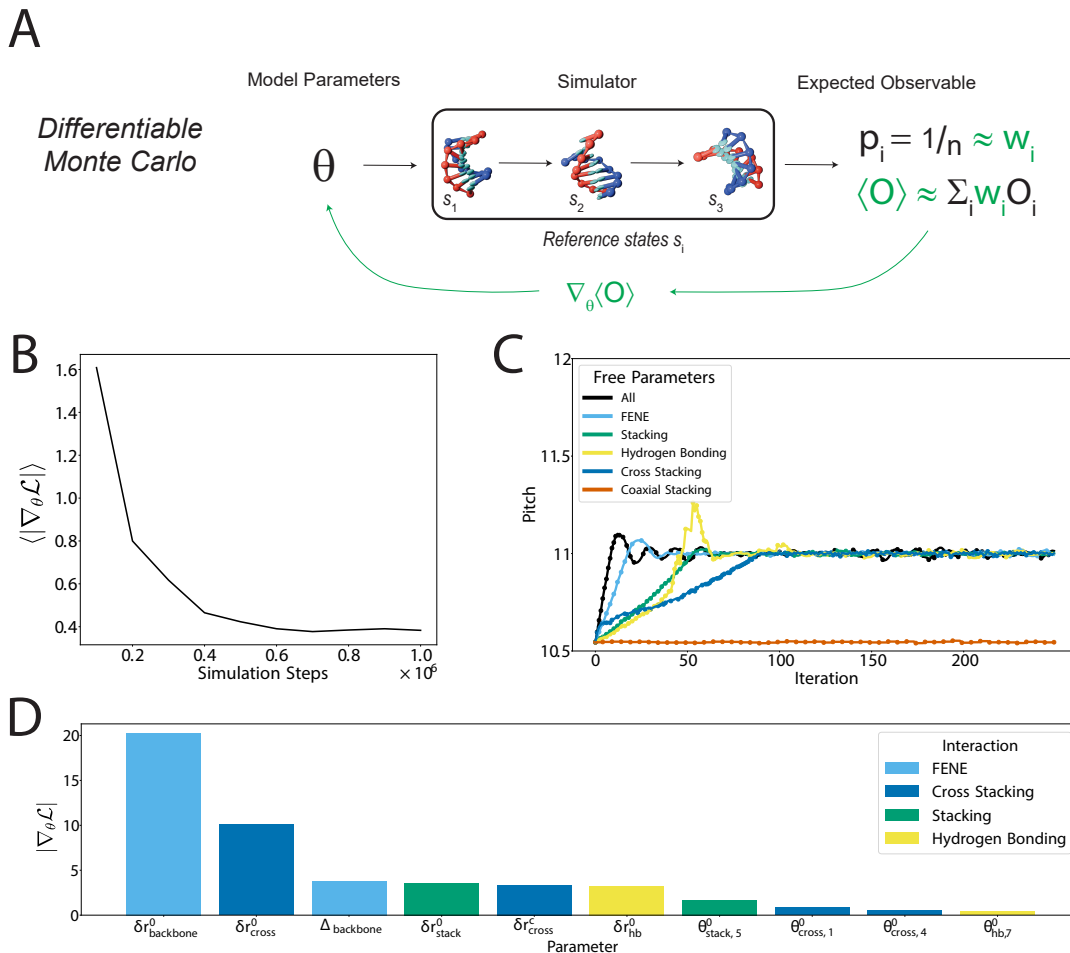


Figure 3: Optimization of oxDNA parameters for target structural properties via trajectory reweighting. **A.** An overview of differentiable Monte Carlo (or “DiffTRE”). **B.** The average absolute value of the gradient as a function of simulation steps when using DiffTRE for stochastic gradient estimation. **C.** The pitch as a function of iteration when using the gradients calculated via DiffTRE for gradient-based optimization. **D.** The ten most significant parameters ranked by the absolute value of their gradients.

We find that for fitting structural properties to oxDNA, DiffTRE provides a numerically stable, scalable, and efficient method for optimization via gradient descent (Figure 3B). Unlike the pathwise and score function estimators, this method yielded oxDNA parameters for specified pitch values within 50 iterations (Figure 3C), and the procedure was stable across various target pitch values. It is important to note that DiffTRE does not require that the sampling procedure itself is differentiable. This means we can optimize oxDNA parameters while using the standalone oxDNA implementation, a highly optimized implementation of the force field, rather than JAX-MD.

For a physics-based model, the gradient estimates for a fixed parameter set contain information about the most important physical interactions for a target property, accessible by ranking parameters based on the magnitude of their gradient (Figure 3D). For pitch, we find that the most significant parameter is the equilibrium distance of the backbone sites, as previously found [37]. More surprisingly, we find that cross-stacking interactions are quite important: this interaction is most often implicated for controlling duplex melting temperatures given its stabilizing role [57, 58, 59]. Sensitivity analysis for propeller twist (Figure S3) also reveals the two most important parameters are involved in the cross-stacking interaction.

Finally, we turn to a sequence-structure pair deposited in Nanobase [60], optimizing the oxDNA parameters to better reproduce the gated DNA nanopore introduced in Ref. [61]. We can choose parameters to minimize the root mean square deviation (RMSD) between the simulated structure and the target structure (Figure S4).

### 2.3 Mechanical Optimization

The second class of data used to fit parameters in oxDNA is mechanical data, e.g. persistence length and stretch and torsional moduli. Computing mechanical properties introduces a host of challenges: while structural properties are typically defined locally and thus only require short ( $\sim 10$  ps) simulations of small (10s of base pairs) systems for convergence, mechanical properties converge over significantly longer time and length scales. For example, oxDNA simulations to compute the persistence length of dsDNA typically require  $\sim 10$   $\mu$ s of simulation time to converge, involving hundreds of nucleotides. Such simulations are well beyond the capabilities of traditional differentiable MD. Second, unlike structural properties, mechanical properties cannot be expressed as an arithmetic mean of state-level observables. Instead, we typically calculate mechanical properties by first calculating a curve representing the ensemble response to force or torque, such as fitting to a worm-like chain model. The parameters from this fit then give summary statistics to match experimental data.

To solve these challenges, we extend DiffTRE to compute derivatives with respect to arbitrary functions of expected observables (Figure 4A) as follows. Consider a set of observables  $\vec{O} = \{O_1, O_2, \dots, O_m\}$  where the  $i^{\text{th}}$  observable corresponds to the response of the system to the  $i^{\text{th}}$  value which one will use to infer an ensemble response, e.g.  $O_i$  corresponds to the extension of a duplex subject to the  $i^{\text{th}}$  value of external force. Given all  $m$  values, we compute the summary statistic of interest  $S$  via an arbitrary line-fitting procedure  $\ell$ , i.e.  $\ell(\vec{O}) = S$ . For control parameters  $\theta$ , we compute  $\nabla_{\theta} S$  by computing an implicit derivative for the line fitting procedure  $\ell$  (see Supporting Information). Figure 4A gives an overview of our procedure, which uses implicit differentiation [62] on the fitting parameters combined with trajectory reweighting, so the entire calculation of mechanical properties becomes end-to-end differentiable. Trajectory reweighting naturally accommodates ensembles involving external forces and torques since their corresponding effect on the probability of a microstate does not depend explicitly on  $\theta$  (see Supporting Information).

As a specific example, under low tension, a long molecule of dsDNA behaves like an extensible wormlike chain (WLC) [63]. In this case, both the persistence length  $L_{ps}$  and the extensional modulus  $S$  are extracted from fits to the WLC expression of Odijk:

$$x = L_0 \left( 1 + \frac{F}{S} - \frac{k_B T}{2F} [1 + y \coth y] \right) \quad (1)$$

with

$$y = \left( \frac{FL_0^2}{L_{ps}k_B T} \right)^{1/2}. \quad (2)$$

Here,  $x$  is the extension of the duplex under force  $F$ ;  $L_0$  is the contour length of the duplex and  $k_B T$  is the thermal energy at temperature  $T$  [64], with  $k_B$  Boltzmann's constant. Thus, given data for a force-extension curve calculated via a set of  $m$  simulations at various forces (i.e. a set of average extensions at  $m$  different forces), we compute  $L_{ps}$ ,  $S$ , and  $L_0$  using an unconstrained three parameter fit to Equation 1. Alternatively,  $L_{ps}$  can be calculated passively via fitting a line to correlations in alignment as a function of separation [65]. Other physical quantities can be treated in a similar fashion: the torsional modulus  $C$ , the effective stretch modulus  $S_{\text{eff}}$ , and the twist-stretch coupling  $g$  require fitting the linear dependence of changes in twist and extension as a function of applied force and torque with analytical formulas derived from the equipartition theorem [24, 66]. Finally, while structural properties are often interpreted as some mean observable of a DNA molecule, the distribution of the same observable can be viewed as a mechanical property [67]; arbitrary probability distributions can be fit to measured distributions and the calculation of summary statistics can similarly be made end-to-end differentiable. See the Supporting Information for details on each of these calculations.

We first apply this method to optimize for  $L_{ps}$  and  $S$ . We find that the most robust fitting procedure is the passive calculation described above (Figure 4B). Although the WLC fit by itself is highly sensitive to details that make optimization more challenging to use directly, we can reduce the variance of the WLC fit and successfully optimize  $S$  by constraining  $L_{ps}$  to the value computed via passive simulations (Figure S5).

Sensitivity analysis again reveals a strong dependence of the persistence length on the cross-stacking interaction; this differs from previous work that has focused on hydrogen-bonding and stacking interactions when fitting new persistence length data [37].

We also optimize the potential for the torsional modulus  $C$  and twist-stretch coupling  $g$  (Figure 4C). Strikingly, our method directly finds a value of  $g$  within experimental uncertainty, requiring the model to capture the transition to

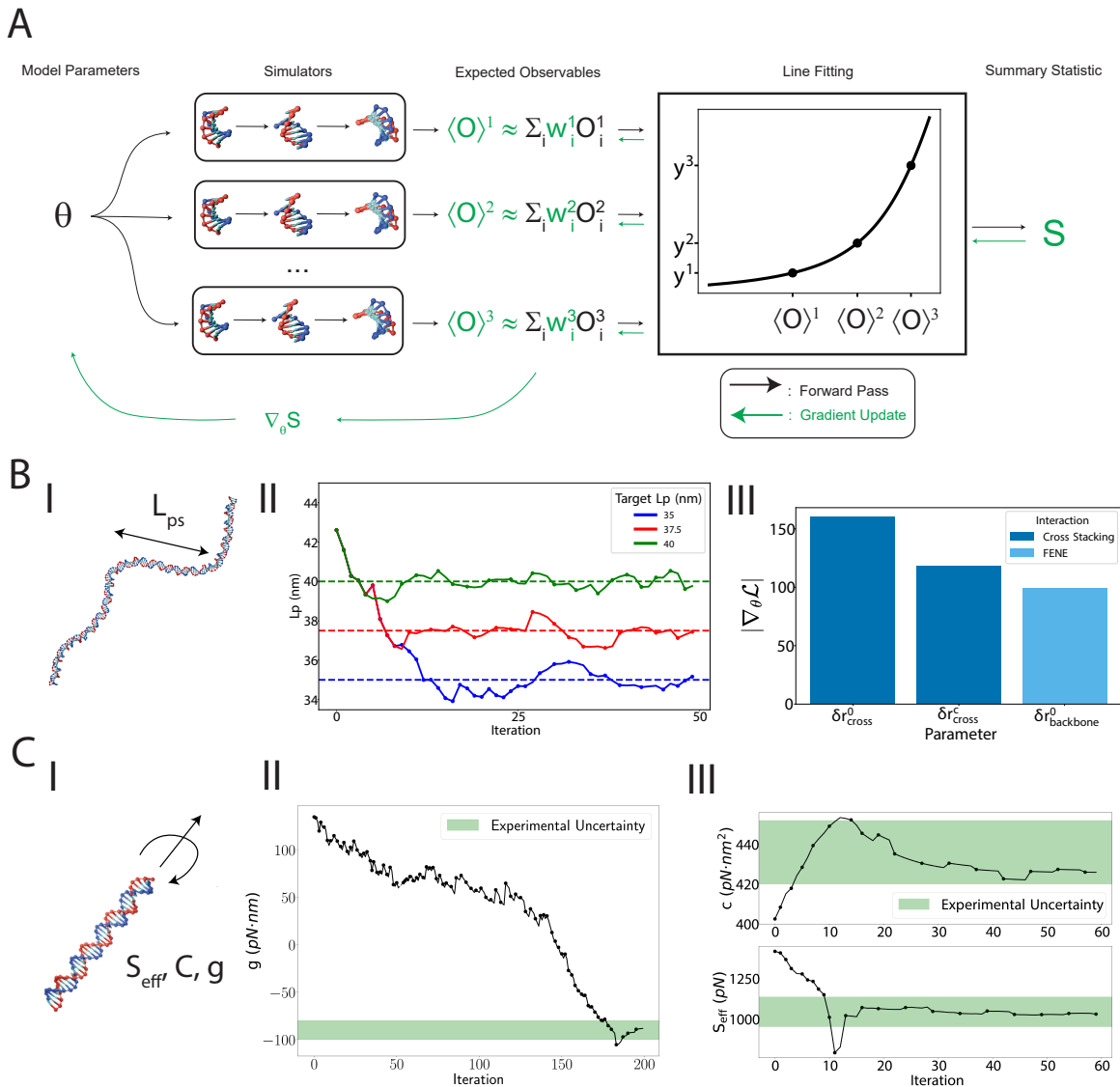


Figure 4: Gradient-based parameter optimization for mechanical properties in oxDNA. **A.** Our method for parameter optimization for complex target mechanical properties via DiffTRE and implicit derivatives. **B.** Parameter optimization for target values of persistence length ( $L_{ps}$ ). **I.** A depiction of  $L_{ps}$ . **II.** Optimization of all oxDNA parameters to match a set target values of  $L_{ps}$ . **III.** The top three most important parameters ranked via the absolute value of the gradient. **C.** Parameter optimization for target values of moduli characterizing response to external force and torque. **I.** A depiction of a duplex under external force and torque. **II-III.** Optimization of all oxDNA parameters to match the twist-stretch coupling, torsional modulus, and effective stretching modulus, all within experimental error. Outliers in the twist-stretch coupling optimization at iterations 52 and 53 are omitted and replaced with a dashed line. See Figure S6 for corresponding sensitivity analyses.

overwinding behavior of dsDNA under low force (Figure 4C.II). This experimental observation previously motivated an entirely new model of DNA [24]. Our fits to  $C$  and  $S_{eff}$  are also within experimental uncertainty (Figure 4C.III). Again, sensitivity analysis reveals a strong dependence of all three quantities on the cross-stacking interaction (Figure S6).

Our method can be further adapted to accommodate additional mechanical properties not explicitly considered in prior oxDNA parameterizations, including those that require jointly optimizing several properties simultaneously. For

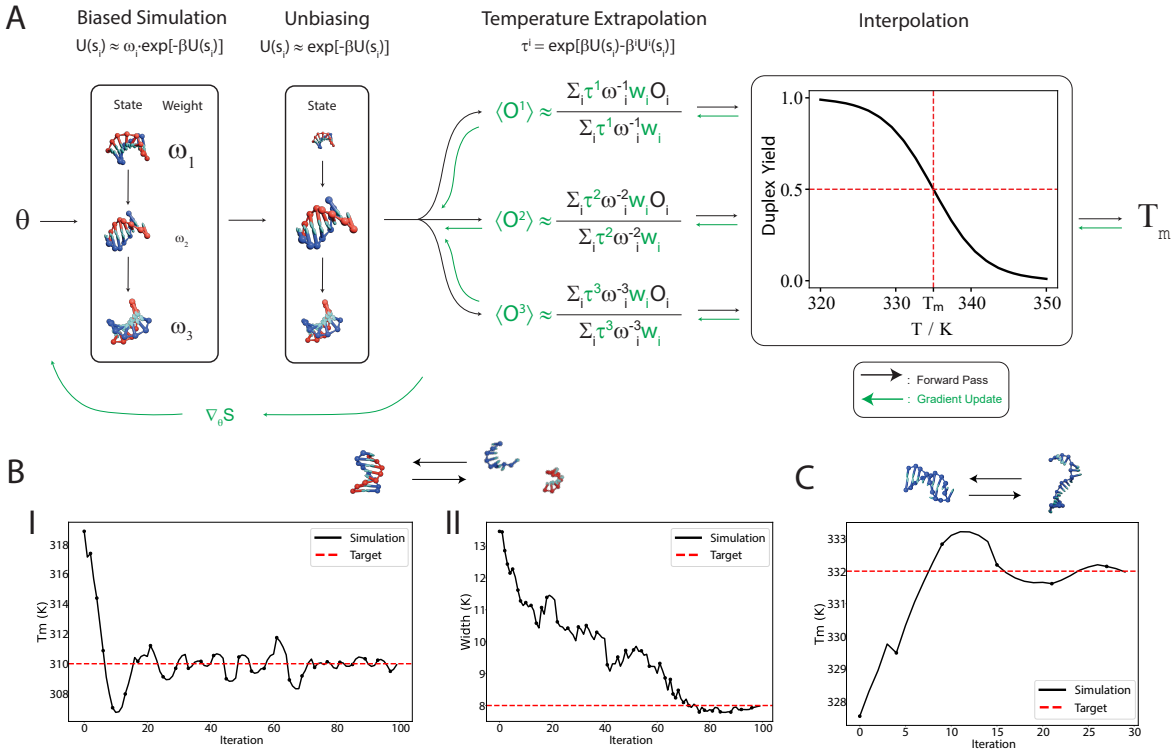


Figure 5: Optimization of oxDNA parameters for target thermodynamic properties. **A**. We perform umbrella sampling via virtual-move Monte Carlo (VMMC) and obtain expected ratios of bound to unbound states at a range of temperature values by reweighting the probability distribution via both the umbrella weight and a weight corresponding to the temperature difference. For the duplex case, we correct these expected ratios via the finite size correction introduced in Ref. [57] (not shown). We then interpolate these ratios to identify the temperature at which there are 50% bound and 50% unbound states. Importantly, the umbrella weights do not depend on  $\theta$  and therefore are not included in the gradient calculation. We apply this scheme to optimize the hydrogen bonding parameters to achieve **B.I**, a melting temperature of  $T_m = 310$  K and **B.II**, a melting transition width of 8 K for an 8 base pair duplex at a salt concentration of 0.5 M with both strands having a total concentration of  $3.3 \times 10^{-4}$  M, and **C**, a melting temperature of  $T_m = 332$  K for a hairpin with a stem length of 6 base pairs and a loop consisting of 6 unpaired nucleotides at a salt concentration of 0.25 M. The duplex and hairpin optimizations are performed using oxDNA1 and oxDNA2, respectively.

example, we optimize for a distribution of propeller twists that maintains a mean value of  $21.7^\circ$  while increasing the variance (Figure S7).

In all optimizations described in this section, we fit the *sequence-averaged* parameters of oxDNA; historically, sequence-specificity is added to oxDNA by separately fitting sequence-specific parameters for the stacking and hydrogen-bonding interactions as multiplicative factors. We additionally fit these parameters to an arbitrarily chosen sequence-specific persistence length (Figure S8), highlighting the flexibility of our method across sequence-averaged and sequence-specific considerations.

## 2.4 Thermodynamic Optimization

The third class of data to which oxDNA is fit is thermodynamic data, i.e. duplex and hairpin melting temperatures. This presents a host of challenges for traditional differentiable MD beyond those discussed so far. First, melting temperatures in oxDNA usually require fitting melting curves to expected values of *discrete* order parameters (i.e. number of base pairs), manifestly not differentiable via the pathwise estimator. Second, melting temperature calculations require enhanced sampling methods such as umbrella sampling, in order to sample sufficient statistics of both bound and unbound structures, and this typically involves non-differentiable cluster-move Monte Carlo schemes. Third, the unbiased

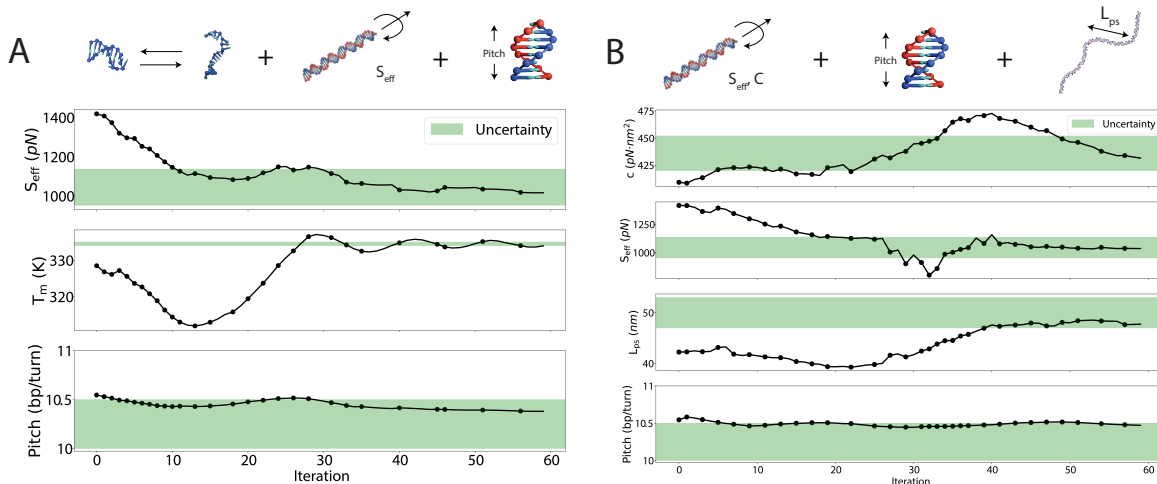


Figure 6: Jointly fitting to multiple target properties simultaneously. **A.** Fitting to  $S_{\text{eff}}$ , pitch, and the  $T_m$  of a hairpin with a 6 nucleotide loop and 6 base-pair stem. The target pitch is  $10.25 \pm 0.25$  bp/turn, the target  $S_{\text{eff}}$  is  $1045 \pm 92$  pN, and the target  $T_m$  is  $334.5 \pm 0.5$  K. **B.** Fitting to  $S_{\text{eff}}$ ,  $C$ , pitch, and  $L_{ps}$  simultaneously. The target  $C$  is  $436 \pm 16$  pN  $\cdot$  nm<sup>2</sup> and the target  $L_{ps}$  is  $42 \pm 2$  nm.

statistics sampled from one biased simulation at a given temperature are then used to extrapolate the corresponding statistics at a range of temperatures, from which a melting curve is finally fit.

We adapt the DiffTRE formalism to accommodate such complex calculations. In umbrella sampling, states  $s_i$  are sampled from a biased Markov chain in which states are sampled with unnormalized probability given by

$$p(s_i) = \omega_i \exp(-\beta U(s_i)) \quad (3)$$

where the weights  $\omega_i$  are chosen to promote configurations along some order parameter(s) that would otherwise be inaccessible to an unweighted Monte Carlo sampling. Similarly, a simulation at temperature  $T$  can be treated as a biased sample of the ensemble at a different temperature  $T'$  and the expected value of a target observable  $O$  at temperature  $T'$  can be computed as

$$\langle O(s) \rangle_{T'} = \langle O(s) \exp(U(s, T)/kT - U(s, T')/kT') \rangle_T \quad (4)$$

Note that this is a special case of Equation 3 where  $\omega_i = \exp(U(s_i, T)/kT)$ . By reformulating the unnormalized probability of a state via Equations 3 and 4, we adapt DiffTRE to differentiate the expected number of base pairs at a given temperature  $T'$ . In practice, we compute the expected ratio of bound to unbound states at each temperature  $T'$  (see Supporting Information). We can then combine these expected ratios with implicit differentiation or simple piecewise interpolation to compute a melting curve and extract  $T_m$ , thus enabling an end-to-end differentiable calculation of  $T_m$ . See Figure 5A for an overview.

We successfully apply our method to optimize melting temperatures of both DNA duplexes and hairpins. Since oxDNA matches Santa-Lucia duplex melting temperatures with high accuracy, we optimize for an arbitrarily different value of  $T_m$  for an 8 base-pair duplex (Figure 5B.I). In principle, we can fit *any* (continuous and differentiable) function of the melting curve. To demonstrate this flexibility, we also fit to an arbitrarily chosen width of the melting curve for the 8 base-pair duplex (Figure 5B.II). Unlike for duplexes, oxDNA underestimates the melting temperatures of hairpins and we therefore fine-tune the parameters to match the melting temperature of a hairpin with a 6 base-pair stem with a loop comprised of 6 unpaired nucleotides as predicted by the Santa-Lucia model (Figure 5C).

Sensitivity analyses for the duplex and hairpin  $T_m$ 's (Figure S9) reveals a pronounced dependence on the cross-stacking interaction; the two most important parameters have gradients 3-4x larger than the next most important parameters. While cross-stacking is generally understood to stabilize duplexes and therefore affect melting, the relative contribution of cross-stacking to hydrogen-bonding and stacking parameters in the model is surprising. Taken together with the sensitivity analyses for structural and mechanical properties, these results suggest that the cross-stacking interaction is far more influential than previously understood in the parameterization of oxDNA.

## 2.5 Joint Optimization

Up until now, we have considered fits to parameter on individual target properties, either structural, mechanical, or thermodynamic. Ideally, fits to oxDNA parameters jointly fit all parameters, allowing the discovery of parameters that fit all experimental properties. To carry this out, we define the objective function as a simple unweighted linear sum of RMSEs for individual properties, though our framework naturally accommodates more sophisticated objective functions (see Supporting Information).

We first apply this to jointly fit  $S_{\text{eff}}$ , pitch, and the  $T_m$  for the hairpin described above. This is motivated by oxDNA’s current overestimate of  $S_{\text{eff}}$  and the difficulty of maintaining structural and thermodynamic properties given strong parameter interdependence. Figure 6A shows the progression of each property throughout the optimization. The optimization begins by decreasing  $S_{\text{eff}}$  within experimental certainty (at the cost of the hairpin  $T_m$ ) and subsequently recovers the hairpin  $T_m$  while maintaining  $S_{\text{eff}}$  and pitch within the specified uncertainty.

Second, we jointly fit  $S_{\text{eff}}$ ,  $C$ ,  $L_p$ , and pitch. This is motivated by difficulty in the original parameterization to capture  $S$  without sacrificing accuracy in other mechanical properties. Figure 6B depicts the progression of each property throughout the optimization, and again we achieve a parameter set that models all properties within the specified uncertainty. Like Figure 6A, the optimization progresses by focusing on a single property at a time (e.g.  $S_{\text{eff}}$ ) at the cost of unoptimized properties (e.g.  $L_{ps}$ ), and then maintaining the optimized properties while proceeding to the next target.

## 3 Discussion

Differentiable programming is an emerging paradigm in scientific computing that holds great promise for bringing the successes of machine-learning to physics-based modelling. However, current methods are limited to relatively simple systems and practitioners have not yet converged on best practices for fitting complex, experimentally-relevant models. In this work, we demonstrate how state-of-the-art methods in differentiable programming can be combined with highly complex simulation routines to fit force field parameters for a well-accepted model of DNA. We successfully optimize structural, mechanical, and thermodynamic properties of DNA. Accomplishing this requires differentiating through simulation methods such as enhanced sampling, external forces and torques, and cluster-move Monte Carlo, as well as downstream calculations such as line-fitting procedures. These methods scale to long simulations of large systems, are both memory-efficient and numerically stable, directly make use of existing molecular simulation software, and permit the joint optimization of several target properties simultaneously.

There is a host of existing numerical methods for fitting coarse-grained force field parameters. For example, methods like force matching, relative entropy minimization, and Boltzmann inversion are often cast as variational problems for deriving coarse-grained potentials. However, each of these methods is limited in its generality. For example, force matching is sensitive to nonlinear dependencies on the force field parameters and therefore the functional form is often restricted to spline interpolation [68]. Similarly, methods like Boltzmann inversion and relative entropy (RE) minimization are effective for matching a ground truth distribution (often derived from atomistic simulations), but the reliance on Lagrange multipliers to constrain ensemble averages (specifically in the case of RE methods) does not accommodate frustrated optimization problems (i.e. those with mutually incompatible data) [69]. In addition, the existing suite of methods cannot be naturally composed, necessitating independent parameter optimizations depending on the applicable method for a given target property. Alternatively, gradient-based methods naturally compose and accommodate frustrated systems. Moreover, gradient-based methods can immediately be integrated with the rich suite of methods developed by the machine learning community for navigating complex optimization landscapes (e.g. momentum-based optimizers, overparameterization via neural networks).

There is also existing work on scaling differentiable MD to complex, experimentally-relevant force fields. Greener uses differentiable simulation with 5 ns trajectories to develop an improved force field for disordered proteins that better reproduces experimentally-measured secondary structure and radius of gyration [49], employing gradient clipping to mitigate the numerical instabilities observed in Figure 2C. Yet, in this formulation, each epoch required one day of compute on 12 GPUs, likely due to the large time cost of differentiating unrolled trajectories (Figure 2D), restricting the optimized parameter set to only five epochs of training. The methods outlined in the present work avoid these difficulties: all optimizations presented in this work were performed on standard high performance computing CPU nodes, and gradient updates take, at most, the duration of the longest forward simulation. This enhanced efficiency permits tens to hundreds of training epochs within several hours or days at low cost.

There are several key limitations of our approach. Foremost, DiffTRE is restricted to ensembles for which unnormalized probabilities of states are known and therefore we only fit to target equilibrium properties. In future work, we plan to exploit fundamental results in non-equilibrium physics (e.g. the Jarzynski equality) to differentiate relevant dynamic properties such as response to external work protocols. In the spirit of actor-critic algorithms in reinforcement learning,

we also envision a more general probabilistic treatment of out-of-equilibrium properties in which the attractor of the dynamical system is parameterized and jointly inferred. There is also great promise in approximate methods of gradient estimation that may enable tractable gradient calculation through unrolled trajectories [70]. A second limitation of our work arises when jointly optimizing for several target properties. In principle, gradients of individual loss terms can conflict, trapping the optimization procedure in local minima. A promising direction to alleviate this limitation is the method introduced by Liu et al. for computing conflict-free update directions given multiple loss terms [71].

There are many additional opportunities for future work. For example, we recently introduced a method for directly designing biopolymers via simulation [72] and our JAX implementation of oxDNA is amenable to this method. Second, existing coarse-grained models are often developed to reproduce models that are themselves approximations, such as the nearest-neighbor model and atomistic simulations. In our framework, one could fit a model of DNA or RNA directly to experimental data (e.g. the optical melting experiments underlying the nearest-neighbor model) rather than the model itself. Finally, we are excited to work with experts in RNA and DNA modelling to fit new coarse-grained models incorporating full datasets of structural, mechanical, and thermodynamic data. Such efforts will benefit from a standardized library of target behavior and corresponding simulation protocols for direct integration with our optimization framework.

## 4 Materials and Methods

Here we provide details on the oxDNA model as well as the method for stochastic gradient estimation given knowledge of unnormalized probabilities developed independently by Zhang et al. [50] and Thaler and Zavadlav [51].

### 4.1 oxDNA

The oxDNA force field is a coarse-grained model of DNA first introduced in 2010 by Thomas Ouldridge [57]. Originally intended to capture DNA properties salient to DNA nanotechnological devices – hybridization, mechanical properties of both single- and double-stranded DNA – oxDNA has since been profitably used in a host of biophysical contexts [73, 74, 75] in addition to becoming a workhorse in the DNA nanotechnology community [40, 54, 60, 76]. The model, widely validated by experiments, has been used to study phenomenon ranging from small-scale strand displacement reactions [41, 44, 45] to the gelation and crystallization of DNA origamis [42, 43, 46, 47]. In its original form, the only sequence specificity in oxDNA was the restriction of hydrogen bonds to valid base pairs (i.e. A-T and G-C). Since its inception, oxDNA has been extended to include base-pair specific hydrogen-bonding and stacking parameters and major and minor grooving. oxDNA has also been tuned to model RNA as well as DNA-RNA interactions.

Under the oxDNA model, DNA is modelled as a string of rigid nucleotides. Each nucleotide is represented as a rigid body consisting of a backbone repulsion site, a stacking site, and a hydrogen-bonding site. All interactions are pairwise and the model considers six types of interactions: backbone connectivity, excluded volume, hydrogen bonding, stacking, cross stacking, and coaxial stacking. More specifically, the potential energy is given by

$$V_{\text{oxdna}} = \sum_{nn} (V_{\text{backbone}} + V_{\text{stack}} + V'_{\text{exc}}) \quad (5)$$

$$+ \sum_{\text{other pairs}} (V_{\text{HB}} + V_{\text{cross\_stack}} + V_{\text{coaxial\_stack}} + V_{\text{exc}}) \quad (6)$$

where  $nn$  denotes the set of consecutive bases within strands. See [57] for details. The latest version of oxDNA, oxDNA 2, contains an additional Debye-Hückel term to model electrostatics. All optimizations presented in this work use the oxDNA 2 model unless otherwise stated.

The parameters of this potential were fit to reproduce three types of properties of single- and double-stranded B-DNA: (i) structural, (ii) mechanical, and (iii) thermodynamic. Examples of structural properties include helical radius, pitch, and propellor twist. Mechanical properties include the persistence length and force-extension properties of both single- and double-stranded DNA, as well as the torsional modulus for the double-stranded case. Regarding thermodynamics, the model is largely fit to reproduce sequence-averaged duplex and hairpin melting temperatures as well as the single-stranded stacking transition. The sequence-averaged parameters of the original model were fit by hand, and the exact properties to which the model was fit versus the properties on which it was evaluated is not recorded.

oxDNA simulations, both in our JAX-MD implementation and the original C++/CUDA implementations, use simulation units as follows [41, 37]: 1 unit force = 48.63 pN; 1 unit time = 3.03 ps; 1 unit temperature = 3000 K; 1 unit energy = 41.42 pN nm. We have used an MD time step of  $dt = 0.005$  simulation units = 15.15 ps for all simulations in this work

with the exception of the sequence-structure optimization in Figure S4, which used  $dt = 0.003$  simulation units = 9.09 ps.

## 4.2 Differentiable Monte Carlo (DiffTRE)

Zhang *et al.* [50] and Thaler and Zavadlav [51] independently developed a method for computing a low variance gradient estimate of an expected value, given knowledge of the unnormalized probabilities of individual samples. For an equilibrium system in the canonical ensemble, the probability of an individual microstate  $\vec{x}_i$  follows the Boltzmann distribution:

$$p(\vec{x}_i) = \frac{e^{-\beta U(\vec{x}_i)}}{Z} \quad (7)$$

where  $\beta$  is the inverse temperature,  $U(\vec{x}_i)$  is the potential energy of  $\vec{x}_i$ , and  $Z = \sum_j e^{-\beta U(\vec{x}_j)}$  is the partition function.

Consider a set of states sampled from this distribution given some control parameters  $\theta$ ,  $X_\theta = \{\vec{x}_1, \vec{x}_2, \dots, \vec{x}_N\}$ , e.g. via standard MD or MC algorithms. The expectation of an arbitrary state-level observable  $O(\vec{x}, \theta)$  is

$$\langle O(\vec{x}, \theta) \rangle_{\vec{x}_i \in X} = \frac{1}{N} \sum_i O(\vec{x}_i, \theta) \quad (8)$$

Following thermodynamic perturbation theory, the key insight is to rewrite Eq. 8 as a weighted sum over sampled states, then adjust this weighting as the governing parameters are changed from reference set  $\hat{\theta}$  to  $\theta$ , assuming sufficient overlap between the respective probability distributions:

$$\langle O(\vec{x}, \theta) \rangle_{\vec{x}_i \in X} = \sum_i w_i O(\vec{x}_i, \theta) \quad (9)$$

where

$$w_i = \frac{p_\theta(\vec{x}_i)/p_{\hat{\theta}}(\vec{x}_i)}{\sum_j p_\theta(\vec{x}_j)/p_{\hat{\theta}}(\vec{x}_j)} \quad (10)$$

and  $\hat{\theta}$  is the reference potential under which  $X_\theta$  was sampled [51]. Crucially, Equation 10 only requires unnormalized probabilities as normalizing factors cancel, e.g. in the case of the canonical ensemble

$$w_i = \frac{e^{-\beta(U_\theta(\vec{x}_i) - U_{\hat{\theta}}(\vec{x}_i))}}{\sum_j e^{-\beta(U_\theta(\vec{x}_j) - U_{\hat{\theta}}(\vec{x}_j))}}, \quad (11)$$

When  $\theta = \hat{\theta}$ , Equation 10 exactly reduces to Equation 8 as  $w_i = \frac{1}{N}$  but  $\nabla_\theta \log(p(\vec{x}_i)) \neq 0$ .

Zhang *et al.* [50] were the first to calculate gradients of expectation values to circumvent full trajectory unrolling in the context of Monte Carlo simulations; Thaler and Zavadlav adapted the approach, which they call ‘differentiable trajectory reweighting (DiffTRE)’, for molecular dynamics simulations [51]. Thaler and Zavadlav also introduced the notion that reference states collected via  $\hat{\theta}$  can be reused for small differences between  $\theta$  and  $\hat{\theta}$ . The effective sample size is

$$N_{\text{eff}} = e^{-\sum_{i=1}^N w_i \ln(w_i)} \quad (12)$$

and, given a total number of reference states  $N_{\text{ref}}$ , reference states are sampled when  $N_{\text{eff}} < \lambda N_{\text{ref}}$  where  $\lambda$  is a hyperparameter.

## Acknowledgments

We thank Petr Sulc Tom Ouldrige, Jonathan Doye, Lorenzo Rovigatti, Erik Poppleton, and Ard Louis for support and helpful discussions surrounding the oxDNA force field and the oxDNA ecosystem. We also thank Petr Sulc and Erik Poppleton for inspiring sequence-structure optimization. We thank Salvatore Assenza and Rubén Pérez for their helpful feedback regarding the calculation of mechanical properties, including providing simulation protocols for stretch-torsion simulations in LAMMPS. We thank Jamie Smith for helpful conversations relating to stochastic gradient estimation. This material is based upon work supported by the NSF AI Institute of Dynamic Systems (#2112085) and the Office of Naval Research (N00014-17-1-3029).



## References

- [1] Ron O. Dror, Robert M. Dirks, J.P. Grossman, Huafeng Xu, and David E. Shaw. Biomolecular Simulation: A Computational Microscope for Molecular Biology. *Annu. Rev. Biophys.*, 41(1):429–452, June 2012.
- [2] Jason D Perlmutter and Michael F Hagan. Mechanisms of virus assembly. *Annual review of physical chemistry*, 66(1):217–239, 2015.
- [3] Roland G Huber, Jan K Marzinek, Daniel A Holdbrook, and Peter J Bond. Multiscale molecular dynamics simulation approaches to the structure and dynamics of viruses. *Progress in Biophysics and Molecular Biology*, 128:121–132, 2017.
- [4] Teresa Ruiz-Herrero and Michael F Hagan. Simulations show that virus assembly and budding are facilitated by membrane microdomains. *Biophysical journal*, 108(3):585–595, 2015.
- [5] Hirotaka Ode, Masaaki Nakashima, Shingo Kitamura, Wataru Sugiura, and Hironori Sato. Molecular dynamics simulation in virus research. *Frontiers in microbiology*, 3:258, 2012.
- [6] Harold A Scheraga, Mey Khalili, and Adam Liwo. Protein-folding dynamics: overview of molecular simulation techniques. *Annu. Rev. Phys. Chem.*, 58(1):57–83, 2007.
- [7] William C Swope, Jed W Pitera, and Frank Suits. Describing protein folding kinetics by molecular dynamics simulations. 1. theory. *The Journal of Physical Chemistry B*, 108(21):6571–6581, 2004.
- [8] Kresten Lindorff-Larsen, Stefano Piana, Ron O Dror, and David E Shaw. How fast-folding proteins fold. *Science*, 334(6055):517–520, 2011.
- [9] Angelo Rosa and Ralf Everaers. Structure and dynamics of interphase chromosomes. *PLoS computational biology*, 4(8):e1000153, 2008.
- [10] Michele Di Pierro, Bin Zhang, Erez Lieberman Aiden, Peter G Wolynes, and José N Onuchic. Transferable model for chromosome architecture. *Proceedings of the National Academy of Sciences*, 113(43):12168–12173, 2016.
- [11] Eva Bertosin, Christopher M. Maffeo, Thomas Drexler, Maximilian N. Honemann, Aleksei Aksimentiev, and Hendrik Dietz. A nanoscale reciprocating rotary mechanism with coordinated mobility control. *Nat Commun*, 12(1):7138, December 2021.
- [12] Anna-Katharina Pumm, Wouter Engelen, Enzo Kopperger, Jonas Isensee, Matthias Vogt, Viktorija Kozina, Massimo Kube, Maximilian N. Honemann, Eva Bertosin, Martin Langecker, Ramin Golestanian, Friedrich C. Simmel, and Hendrik Dietz. A DNA origami rotary ratchet motor. *Nature*, 607(7919):492–498, July 2022.
- [13] Sanjay Kosara, Ramesh Singh, and Dhiraj Bhatia. Structural dna nanotechnology at the nexus of next-generation bio-applications: challenges and perspectives. *Nanoscale Adv.*, 6:386–401, 2024.
- [14] Josh Achiam, Steven Adler, Sandhini Agarwal, Lama Ahmad, Ilge Akkaya, Florencia Leoni Aleman, Diogo Almeida, Janko Altschmidt, Sam Altman, Shyamal Anadkat, et al. Gpt-4 technical report. *arXiv preprint arXiv:2303.08774*, 2023.
- [15] Gemini Team, Petko Georgiev, Ving Ian Lei, Ryan Burnell, Libin Bai, Anmol Gulati, Garrett Tanzer, Damien Vincent, Zhufeng Pan, Shibo Wang, et al. Gemini 1.5: Unlocking multimodal understanding across millions of tokens of context. *arXiv preprint arXiv:2403.05530*, 2024.
- [16] John Jumper, Richard Evans, Alexander Pritzel, Tim Green, Michael Figurnov, Olaf Ronneberger, Kathryn Tunyasuvunakool, Russ Bates, Augustin Židek, Anna Potapenko, et al. Highly accurate protein structure prediction with alphafold. *nature*, 596(7873):583–589, 2021.
- [17] David Donoho. Data science at the singularity. *Harvard Data Science Review*, 6(1), 2024.
- [18] Thomas E. Ouldridge, Ard A. Louis, and Jonathan P. K. Doye. Structural, mechanical, and thermodynamic properties of a coarse-grained DNA model. *The Journal of Chemical Physics*, 134(8):085101, February 2011.
- [19] Tiedong Sun, Vishal Minhas, Nikolay Korolev, Alexander Mirzoev, Alexander P Lyubartsev, and Lars Nordenskiöld. Bottom-up coarse-grained modeling of dna. *Frontiers in Molecular Biosciences*, 8:645527, 2021.
- [20] Sweta Vangaveti, Srivathsan V Ranganathan, and Alan A Chen. Advances in rna molecular dynamics: a simulator’s guide to rna force fields. *Wiley Interdisciplinary Reviews: RNA*, 8(2):e1396, 2017.
- [21] Alberto Pérez, F Javier Luque, and Modesto Orozco. Frontiers in molecular dynamics simulations of dna. *Accounts of chemical research*, 45(2):196–205, 2012.
- [22] Dazhi Tan, Stefano Piana, Robert M Dirks, and David E Shaw. Rna force field with accuracy comparable to state-of-the-art protein force fields. *Proceedings of the National Academy of Sciences*, 115(7):E1346–E1355, 2018.

- [23] Thomas A Knotts, Nitin Rathore, David C Schwartz, and Juan J De Pablo. A coarse grain model for dna. *The Journal of chemical physics*, 126(8), 2007.
- [24] Salvatore Assenza and Rubén Pérez. Accurate Sequence-Dependent Coarse-Grained Model for Conformational and Elastic Properties of Double-Stranded DNA. *J. Chem. Theory Comput.*, 18(5):3239–3256, May 2022.
- [25] Daniel M. Hinckley, Gordon S. Freeman, Jonathan K. Whitmer, and Juan J. de Pablo. An experimentally-informed coarse-grained 3-site-per-nucleotide model of DNA: Structure, thermodynamics, and dynamics of hybridization. *J. Chem. Phys.*, 139(14):144903, October 2013.
- [26] Gordon S. Freeman, Daniel M. Hinckley, Joshua P. Lequieu, Jonathan K. Whitmer, and Juan J. de Pablo. Coarse-grained modeling of DNA curvature. *The Journal of Chemical Physics*, 141(16):165103, October 2014.
- [27] Debayan Chakraborty, Naoto Hori, and D. Thirumalai. Sequence-Dependent Three Interaction Site Model for Single- and Double-Stranded DNA. *J. Chem. Theory Comput.*, 14(7):3763–3779, July 2018.
- [28] Pablo D. Dans, Ari Zeida, Matías R. Machado, and Sergio Pantano. A Coarse Grained Model for Atomic-Detailed DNA Simulations with Explicit Electrostatics. *J. Chem. Theory Comput.*, 6(5):1711–1725, May 2010.
- [29] Pablo D Dans, Jürgen Walther, Hansel Gómez, and Modesto Orozco. Multiscale simulation of DNA. *Current Opinion in Structural Biology*, 37:29–45, April 2016.
- [30] Jaakko J. Uusitalo, Helgi I. Ingólfsson, Parisa Akhshi, D. Peter Tieleman, and Siewert J. Marrink. Martini Coarse-Grained Force Field: Extension to DNA. *J. Chem. Theory Comput.*, 11(8):3932–3945, August 2015.
- [31] Christopher Maffeo, Thuy T. M. Ngo, Taekjip Ha, and Aleksei Aksimentiev. A Coarse-Grained Model of Unstructured Single-Stranded DNA Derived from Atomistic Simulation and Single-Molecule Experiment. *J. Chem. Theory Comput.*, 10(8):2891–2896, August 2014.
- [32] Yi He, Adam Liwo, and Harold A. Scheraga. Optimization of a Nucleic Acids united-RESidue 2-Point model (NARES-2P) with a maximum-likelihood approach. *The Journal of Chemical Physics*, 143(24):243111, December 2015.
- [33] Aymeric Naômé, Aatto Laaksonen, and Daniel P. Vercauteren. A Solvent-Mediated Coarse-Grained Model of DNA Derived with the Systematic Newton Inversion Method. *J. Chem. Theory Comput.*, 10(8):3541–3549, August 2014.
- [34] Petr Šulc, Flavio Romano, Thomas E Ouldridge, Lorenzo Rovigatti, Jonathan PK Doye, and Ard A Louis. Sequence-dependent thermodynamics of a coarse-grained dna model. *The Journal of chemical physics*, 137(13), 2012.
- [35] Petr Šulc, Flavio Romano, Thomas E Ouldridge, Jonathan PK Doye, and Ard A Louis. A nucleotide-level coarse-grained model of rna. *The Journal of chemical physics*, 140(23), 2014.
- [36] Jonah Procyk, Erik Poppleton, and Petr Šulc. Coarse-grained nucleic acid–protein model for hybrid nanotechnology. *Soft Matter*, 17(13):3586–3593, 2021.
- [37] Benedict EK Snodin, Ferdinando Randisi, Majid Mosayebi, Petr Šulc, John S Schreck, Flavio Romano, Thomas E Ouldridge, Roman Tsukanov, Eyal Nir, Ard A Louis, et al. Introducing improved structural properties and salt dependence into a coarse-grained model of dna. *The Journal of chemical physics*, 142(23), 2015.
- [38] Eryk J Ratajczyk, Petr Šulc, Andrew J Turberfield, Jonathan PK Doye, and Ard A Louis. Coarse-grained modeling of dna–rna hybrids. *The Journal of Chemical Physics*, 160(11), 2024.
- [39] Jonathan PK Doye, Hannah Fowler, Domen Prešern, Joakim Bohlin, Lorenzo Rovigatti, Flavio Romano, Petr Šulc, Chak Kui Wong, Ard A Louis, John S Schreck, et al. The oxdna coarse-grained model as a tool to simulate dna origami. In *DNA and RNA Origami: Methods and Protocols*, pages 93–112. Springer, 2023.
- [40] Aditya Sengar, Thomas E Ouldridge, Oliver Henrich, Lorenzo Rovigatti, and P Šulc. A primer on the oxdna model of dna: when to use it, how to simulate it and how to interpret the results. *Frontiers in Molecular Biosciences*, 8:693710, 2021.
- [41] Thomas E Ouldridge, Ard A Louis, and Jonathan PK Doye. Dna nanotweezers studied with a coarse-grained model of dna. *Physical Review Letters*, 104(17):178101, 2010.
- [42] Lorenzo Rovigatti, Frank Smallegang, Flavio Romano, and Francesco Sciortino. Gels of dna nanostars never crystallize. *ACS nano*, 8(4):3567–3574, 2014.
- [43] Flavio Romano and Francesco Sciortino. Switching bonds in a dna gel: An all-dna vitrimer. *Physical Review Letters*, 114(7):078104, 2015.

- [44] Robert RF Machinek, Thomas E Ouldridge, Natalie EC Haley, Jonathan Bath, and Andrew J Turberfield. Programmable energy landscapes for kinetic control of dna strand displacement. *Nature communications*, 5(1):5324, 2014.
- [45] Natalie EC Haley, Thomas E Ouldridge, Ismael Mullor Ruiz, Alessandro Geraldini, Ard A Louis, Jonathan Bath, and Andrew J Turberfield. Design of hidden thermodynamic driving for non-equilibrium systems via mismatch elimination during dna strand displacement. *Nature communications*, 11(1):2562, 2020.
- [46] Hao Liu, Michael Matthies, John Russo, Lorenzo Rovigatti, Raghu Pradeep Narayanan, Thong Diep, Daniel McKeen, Oleg Gang, Nicholas Stephanopoulos, Francesco Sciortino, et al. Inverse design of a pyrochlore lattice of dna origami through model-driven experiments. *Science*, 384(6697):776–781, 2024.
- [47] Mathias Centola, Erik Poppleton, Sujay Ray, Martin Centola, Robb Welty, Julián Valero, Nils G Walter, Petr Šulc, and Michael Famulok. A rhythmically pulsing leaf-spring dna-origami nanoengine that drives a passive follower. *Nature nanotechnology*, 19(2):226–236, 2024.
- [48] Luke Metz, C Daniel Freeman, Samuel S Schoenholz, and Tal Kachman. Gradients are not all you need. *arXiv preprint arXiv:2111.05803*, 2021.
- [49] Joe G Greener. Differentiable simulation to develop molecular dynamics force fields for disordered proteins. *Chemical Science*, 15(13):4897–4909, 2024.
- [50] Shi-Xin Zhang, Zhou-Quan Wan, and Hong Yao. Automatic differentiable monte carlo: Theory and application. *Physical Review Research*, 5(3):033041, 2023.
- [51] Stephan Thaler and Julija Zavadlav. Learning neural network potentials from experimental data via differentiable trajectory reweighting. *Nature communications*, 12(1):6884, 2021.
- [52] James Bradbury, Roy Frostig, Peter Hawkins, Matthew James Johnson, Chris Leary, Dougal Maclaurin, George Necula, Adam Paszke, Jake VanderPlas, Skye Wanderman-Milne, and Qiao Zhang. JAX: composable transformations of Python+NumPy programs, 2018.
- [53] Samuel Schoenholz and Ekin Dogus Cubuk. Jax md: a framework for differentiable physics. *Advances in Neural Information Processing Systems*, 33:11428–11441, 2020.
- [54] Erik Poppleton, Michael Matthies, Debesh Mandal, Flavio Romano, Petr Šulc, and Lorenzo Rovigatti. oxdna: coarse-grained simulations of nucleic acids made simple. *Journal of Open Source Software*, 8(81):4693, 2023.
- [55] Lorenzo Rovigatti, Petr Šulc, István Z Reguly, and Flavio Romano. A comparison between parallelization approaches in molecular dynamics simulations on gpus. *Journal of computational chemistry*, 36(1):1–8, 2015.
- [56] Oliver Henrich, Yair Augusto Gutiérrez Fosado, Tine Curk, and Thomas E Ouldridge. Coarse-grained simulation of dna using lammmps: An implementation of the oxdna model and its applications. *The European Physical Journal E*, 41:1–16, 2018.
- [57] Thomas E Ouldridge. *Coarse-grained modelling of DNA and DNA self-assembly*. Springer Science & Business Media, 2012.
- [58] Marcel Swart, Tushar van der Wijst, Célia Fonseca Guerra, and F Matthias Bickelhaupt.  $\pi$ - $\pi$  stacking tackled with density functional theory. *Journal of molecular modeling*, 13:1245–1257, 2007.
- [59] Jiří Šponer, Petr Jurečka, Ivan Marchan, F Javier Luque, Modesto Orozco, and Pavel Hobza. Nature of base stacking: reference quantum-chemical stacking energies in ten unique b-dna base-pair steps. *Chemistry—A European Journal*, 12(10):2854–2865, 2006.
- [60] Erik Poppleton, Aatmik Mallya, Swarup Dey, Joel Joseph, and Petr Šulc. Nanobase. org: a repository for dna and rna nanostructures. *Nucleic acids research*, 50(D1):D246–D252, 2022.
- [61] Jonathan R Burns, Astrid Seifert, Niels Fertig, and Stefan Howorka. A biomimetic dna-based channel for the ligand-controlled transport of charged molecular cargo across a biological membrane. *Nature nanotechnology*, 11(2):152–156, 2016.
- [62] Mathieu Blondel, Quentin Berthet, Marco Cuturi, Roy Frostig, Stephan Hoyer, Felipe Llinares-López, Fabian Pedregosa, and Jean-Philippe Vert. Efficient and modular implicit differentiation. *Advances in neural information processing systems*, 35:5230–5242, 2022.
- [63] John F Marko and Eric D Siggia. Stretching dna. *Macromolecules*, 28(26):8759–8770, 1995.
- [64] Theo Odijk. Stiff chains and filaments under tension. *Macromolecules*, 28(20):7016–7018, 1995.
- [65] Charles R Cantor and Paul Reinhard Schimmel. *Biophysical chemistry: Part III: the behavior of biological macromolecules*. Macmillan, 1980.

- [66] Alberto S Sassi, Salvatore Assenza, and Paolo De Los Rios. Shape of a stretched polymer. *Physical review letters*, 119(3):037801, 2017.
- [67] D Petkevičiūtė, M Pasi, O Gonzalez, and JH Maddocks. cgdna: a software package for the prediction of sequence-dependent coarse-grain free energies of b-form dna. *Nucleic acids research*, 42(20):e153–e153, 2014.
- [68] Sergei Izvekov and Gregory A Voth. A multiscale coarse-graining method for biomolecular systems. *The Journal of Physical Chemistry B*, 109(7):2469–2473, 2005.
- [69] Andrea Cesari, Sabine Reißer, and Giovanni Bussi. Using the maximum entropy principle to combine simulations and solution experiments. *Computation*, 6(1):15, 2018.
- [70] Deniz Oktay, Nick McGreivy, Joshua Aduol, Alex Beatson, and Ryan P Adams. Randomized automatic differentiation. *arXiv preprint arXiv:2007.10412*, 2020.
- [71] Qiang Liu, Mengyu Chu, and Nils Thuerey. Config: Towards conflict-free training of physics informed neural networks. *arXiv preprint arXiv:2408.11104*, 2024.
- [72] Ryan Krueger, Michael P Brenner, and Krishna Shrinivas. Generalized design of sequence-ensemble-function relationships for intrinsically disordered proteins. *bioRxiv*, pages 2024–10, 2024.
- [73] Majid Mosayebi, Flavio Romano, Thomas E. Ouldridge, Ard A. Louis, and Jonathan P. K. Doye. The Role of Loop Stacking in the Dynamics of DNA Hairpin Formation. *J. Phys. Chem. B*, 118(49):14326–14335, December 2014.
- [74] John S. Schreck, Thomas E. Ouldridge, Flavio Romano, Petr Šulc, Liam P. Shaw, Ard A. Louis, and Jonathan P.K. Doye. DNA hairpins destabilize duplexes primarily by promoting melting rather than by inhibiting hybridization. *Nucleic Acids Res.*, 43(13):6181–6190, July 2015.
- [75] Stefanos K. Nomidis, Enrico Skoruppa, Enrico Carlon, and John F. Marko. Twist-bend coupling and the statistical mechanics of the twistable wormlike-chain model of dna: Perturbation theory and beyond. *Phys. Rev. E*, 99:032414, Mar 2019.
- [76] Thomas E Ouldridge. Dna nanotechnology: understanding and optimisation through simulation. *Molecular Physics*, 113(1):1–15, 2015.
- [77] Shakir Mohamed, Mihaela Rosca, Michael Figurnov, and Andriy Mnih. Monte carlo gradient estimation in machine learning. *The Journal of Machine Learning Research*, 21(1):5183–5244, 2020.
- [78] Megan C Engel, Jamie A Smith, and Michael P Brenner. Optimal control of nonequilibrium systems through automatic differentiation. *Physical Review X*, 13(4):041032, 2023.
- [79] Ruslan L Davidchack, TE Ouldridge, and MV Tretyakov. New langevin and gradient thermostats for rigid body dynamics. *The Journal of chemical physics*, 142(14), 2015.
- [80] Benedict Leimkuhler and Charles Matthews. Rational construction of stochastic numerical methods for molecular sampling. *Applied Mathematics Research eXpress*, 2013(1):34–56, 2013.
- [81] Erik Poppleton, Joakim Bohlin, Michael Matthies, Shuchi Sharma, Fei Zhang, and Petr Šulc. Design, optimization and analysis of large dna and rna nanostructures through interactive visualization, editing and molecular simulation. *Nucleic acids research*, 48(12):e72–e72, 2020.
- [82] Philipp Moritz, Robert Nishihara, Stephanie Wang, Alexey Tumanov, Richard Liaw, Eric Liang, Melih Elibol, Zongheng Yang, William Paul, Michael I Jordan, et al. Ray: A distributed framework for emerging {AI} applications. In *13th USENIX symposium on operating systems design and implementation (OSDI 18)*, pages 561–577, 2018.
- [83] Zev Bryant, Michael D. Stone, Jeff Gore, Steven B. Smith, Nicholas R. Cozzarelli, and Carlos Bustamante. Structural transitions and elasticity from torque measurements on DNA. *Nature*, 424(6946):338–341, July 2003.
- [84] Jeff Gore, Zev Bryant, Marcelo Nöllmann, Mai U. Le, Nicholas R. Cozzarelli, and Carlos Bustamante. DNA overwinds when stretched. *Nature*, 442(7104):836–839, August 2006.

## A Preliminaries

### A.1 Stochastic Gradient Estimation

The challenge of computing the gradient of an expectation with respect to the parameters defining the distribution over which it is integrated is a well-explored topic in machine learning literature (for an in-depth review, refer to [77]). Consider a loss function  $\mathcal{L}(\theta)$  defined as:

$$\mathcal{L}(\theta) := \int p(x; \theta) O(x; \theta) dx = \mathbb{E}_{p(x; \theta)} [f(x; \theta)] \quad (13)$$

Here,  $p(x; \theta)$  denotes a probability distribution over a random variable  $x$  that depends on the parameter  $\theta$ , and  $O(x; \theta)$  represents an observable of interest. For instance, in minimizing the RMSD between a measured helical diameter with a target value,  $O(x; \theta)$  could represent the helical diameter for a particular configuration, and  $\mathcal{L}(\theta)$  captures the difference between the target value and the expected diameter over an ensemble of such configurations.

Optimizing  $\mathcal{L}(\theta)$  often requires computing its gradient:

$$\nabla_{\theta} \mathcal{L}(\theta) = \nabla_{\theta} \left( \int p(x; \theta) O(x; \theta) dx \right) \quad (14)$$

$$= \int p(x; \theta) \nabla_{\theta} O(x; \theta) dx + \int \nabla_{\theta} p(x; \theta) O(x; \theta) dx \quad (15)$$

$$= \mathbb{E}_{p(x; \theta)} [\nabla_{\theta} O(x; \theta)] + \mathbb{E}_{p(x; \theta)} [\nabla_{\theta} \log p(x; \theta) O(x; \theta)] \quad (16)$$

via the identity  $\nabla_{\theta} p(x; \theta) = p(x; \theta) \nabla_{\theta} \log p(x; \theta)$ . In standard supervised learning, random sampling of training examples ensures that  $\nabla_{\theta} \log p(x; \theta) = 0$  and simplifies the gradient to  $\mathbb{E}_{p(x; \theta)} [\nabla_{\theta} O(x; \theta)]$ . Conversely, in reinforcement learning, the distribution  $p(x; \theta)$  – determined by the policy – is parameter-dependent, but the observable  $O(x; \theta)$  is usually not. To address this, the gradient is often reparameterized to isolate the source of randomness. In the *pathwise gradient estimator*, samples  $x$  are generated from a distribution  $q_{\epsilon}(\theta)$ , independent of  $\theta$ , and are mapped deterministically to  $x(\epsilon; \theta)$ . This results in:

$$\nabla_{\theta} \mathcal{L}(\theta) = \mathbb{E}_{p(\epsilon)} [\nabla_{\theta} O(x(\epsilon; \theta))] \quad (17)$$

This approach, known as the *reparameterization trick*, allows the gradient to be computed as if it were a supervised learning problem. Alternatively, reinforcement learning employs the score-function gradient estimator:

$$\nabla_{\theta} \mathcal{L}(\theta) = \mathbb{E}_{p(x; \theta)} [\nabla_{\theta} \log p(x; \theta) O(x; \theta)] \quad (18)$$

Commonly known as the REINFORCE algorithm [77], this formulation provides a signal that increases the probability of high-value states and decreases the probability of low-value ones.

Each gradient estimation technique comes with its own advantages and limitations. The reparameterization trick is beneficial when the function or system being optimized can be differentiated through its entire process, allowing for gradient estimation that resembles standard backpropagation in supervised learning. This approach often results in lower variance estimates and more efficient optimization. However, its main drawback is the requirement for a differentiable path through the process, which may not always be feasible for complex or discrete simulations. On the other hand, the score-function estimator (REINFORCE algorithm) provides more flexibility, as it only requires differentiating the probability distribution itself, making it applicable in cases where direct differentiation through the process is impossible. The trade-off, however, is that this method often has higher variance, which can lead to less stable and slower convergence during optimization.

### A.2 Differentiable Molecular Dynamics

In standard molecular dynamics simulations, a system comprising  $n$  interacting particles, represented by a vector  $\mathbf{x} \in \mathcal{R}^{6n}$  that encodes their positions and momenta, is propagated iteratively over time using an integration step function  $\mathcal{S}$ :

$$\mathbf{x}_{t+1} = \mathcal{S}(\mathbf{x}_t, \theta)$$

Here,  $\mathcal{S}$  is defined by the energy function and the numerical integration method, with  $\theta$  representing control parameters. For a given number of steps  $N$ , the final state  $\mathbf{x}_N$  can be represented via a single function evaluation:

$$\mathcal{T}(\mathbf{x}_0) \equiv \mathcal{S}(\cdots \mathcal{S}(\mathcal{S}(\mathbf{x}_0)) \cdots) = \mathbf{x}_N \quad (19)$$

where  $\mathcal{S}$  is applied  $N$  times and  $\mathbf{x}_0$  is the initial state. This implies that an MD trajectory can be represented as the result of one numerical computation.

When embedded within an automatic differentiation framework, gradients of this computation can be efficiently computed with respect to  $\theta$ . Assume an objective function dependent on the final state  $\mathbf{x}_N$  and control parameters  $\theta$ , denoted  $O(\mathbf{x}_N, \theta)$ . Given the stochastic nature of MD trajectories, the common objective is the expectation of such functions:

$$\mathcal{L}(\theta) \equiv \langle O(\mathbf{x}_N, \theta) \rangle_{\rho \in \mathbb{R}} = \langle O(\mathcal{T}(\mathbf{x}_0), \theta) \rangle_{\rho \in \mathbb{R}} \quad (20)$$

$$= \frac{1}{|\mathbb{R}|} \sum_{\rho \in \mathbb{R}} O(\mathcal{T}_\rho(\mathbf{x}_0), \theta) \quad (21)$$

where  $\mathbb{R}$  represents a set of random seeds initializing the trajectories and  $\mathbf{x}_{N,\rho}$  is the final state for seed  $\rho \in \mathbb{R}$ . Gradients are typically computed via the reparameterization trick (c.f. [78]):

$$\nabla_\theta \mathcal{L}(\theta) \approx \langle \nabla_\theta O(\mathcal{T}_\rho(\mathbf{x}_0), \theta) \rangle_{\rho \in \mathbb{R}} \quad (22)$$

It is important to note that (i) objective functions can also be defined to depend on the entire trajectory rather than solely on the final state, and (ii) in equilibrium systems with long simulations, states separated by sufficiently large time intervals can be interpreted as distinct trajectories under standard assumptions of ergodicity. However, for clarity, this discussion will focus on current formulations.

Since gradients must be computed while considering the simulation process, which requires repeated application of  $\mathcal{S}$ , computational and memory limitations may arise. To illustrate, consider the gradient in Equation 22 for one-dimensional space (see Ref. [48] for details):

$$\frac{dO_N}{d\theta} = \frac{\partial O_N}{\partial \theta} + \sum_{k=1}^N \frac{\partial O_N}{\partial \mathbf{x}_N} \left( \prod_{i=k}^N \frac{\partial \mathbf{x}_i}{\partial \mathbf{x}_{i-1}} \right) \frac{\partial \mathbf{x}_k}{\partial \theta} \quad (23)$$

where  $O_N$  is the objective function evaluated at the final state. A critical aspect here is the Jacobian of the dynamical system, represented by the matrix of partial derivatives  $\frac{\partial \mathbf{x}_i}{\partial \mathbf{x}_{i-1}}$ . The magnitude of the Jacobian's eigenvalues must generally be less than one for the gradient calculation to be stable.

### A.3 Implicit Differentiation

The typical paradigm in differentiable programming is to treat a program as an analytical calculation that is subject to the chain rule. However, complications arise for iterative programs such as optimization algorithms (e.g. line fitting procedures). Optimization algorithms can not typically be represented as an explicit formula in terms of their inputs; instead, one must differentiate through an unrolled iterative procedure, which imposes significant numerical and memory issues, or apply heuristics such as using the final iteration as a proxy for the optimization problem solution.

An alternative approach to differentiate through optimization procedures is to implicitly relate the solution of an optimization problem to its inputs using optimality conditions. Consider an optimization procedure  $y : \mathbb{R}^n \rightarrow \mathbb{R}^m$  that maps an input  $x \in \mathbb{R}^n$  to a solution  $y(x) \in \mathbb{R}^m$  that satisfies an optimality condition described by the relation  $R(y(x), x) = 0$ . When the relation  $R$  is continuously differentiable and  $\partial R_y$  evaluated at  $(y(x), x)$  is square invertible, the implicit function theorem provides expression for the implicit relationship between  $x$  and  $y(x)$ :

$$\partial_x y(x) = \frac{\partial R_x(y(x), x)}{\partial R_y(y(x), x)} \quad (24)$$

Crucially, Equation 24 provides an alternative means of computing  $\partial_x y(x)$  to unrolling  $y$  that is exact while numerically and computationally stable.

Historically, this approach required complicated, case-specific derivations that made implicit differentiation difficult to use in practice. However, Blondel et al. [62] developed a method for automatic implicit differentiation that uses automatic differentiation to compute  $\partial_x y(x)$  without deriving  $\partial R_x(y(x), x)$  and  $\partial R_y(y(x), x)$  by hand. We use this method in this work to compute derivatives of line fitting procedures involved in the calculation of thermodynamic and mechanical properties of DNA.

## B Notation

For a given topology (i.e. a set of bonded pairs), an oxDNA configuration of  $n$  nucleotides is represented in a space-fixed frame by the center of masses of each nucleotide,  $\mathbf{R} \in \mathbb{R}^{n \times 3}$ , and the orientations of each particle represented by a quaternion,  $\mathbf{Q} \in \mathbb{R}^{n \times 4}$ . For a given nucleotide, a local reference frame can also be defined with basis vectors  $\mathbf{a}_1$  (a vector directed from the backbone site to the base site),  $\mathbf{a}_2$  (a vector normal to the plane of the base), and  $\mathbf{a}_3$  ( $\mathbf{a}_3 = \mathbf{a}_1 \times \mathbf{a}_2$ ). For the  $i^{\text{th}}$  nucleotide with orientation described by  $\mathbf{q} = \mathbf{Q}_i \in \mathbb{R}^4$ , the local nucleotide reference frame can be computed as:

$$\mathbf{a}_1 = [q_0^2 + q_1^2 - q_2^2 - q_3^2, 2(q_1 q_2 + q_0 q_3), 2(q_1 q_3 - q_0 q_2)] \quad (25)$$

$$\mathbf{a}_2 = [2(q_1 q_2 - q_0 q_3), q_0^2 - q_1^2 + q_2^2 - q_3^2, 2(q_2 q_3 + q_0 q_1)] \quad (26)$$

$$\mathbf{a}_3 = [2(q_1 q_3 + q_0 q_2), 2(q_2 q_3 - q_0 q_1), q_0^2 - q_1^2 - q_2^2 + q_3^2] \quad (27)$$

In oxDNA, a nucleotide has three interaction sites used in the energy calculation – a backbone repulsion site, a stacking site, and a hydrogen bonding site. For a particular nucleotide with centre of mass  $\mathbf{r} = \mathbf{R}_i \in \mathbb{R}^3$ , the locations of these interaction sites in the *space-fixed frame* are given by:

$$\mathbf{r}_{\text{back}} = \mathbf{r} + d_{1,\text{back}}\mathbf{a}_1 + d_{2,\text{back}}\mathbf{a}_2 + d_{3,\text{back}}\mathbf{a}_3 \quad (28)$$

$$\mathbf{r}_{\text{stack}} = \mathbf{r} + d_{1,\text{stack}}\mathbf{a}_1 + d_{2,\text{stack}}\mathbf{a}_2 + d_{3,\text{stack}}\mathbf{a}_3 \quad (29)$$

$$\mathbf{r}_{\text{hb}} = \mathbf{r} + d_{1,\text{hb}}\mathbf{a}_1 + d_{2,\text{hb}}\mathbf{a}_2 + d_{3,\text{hb}}\mathbf{a}_3 \quad (30)$$

$$(31)$$

where vectors  $\mathbf{d}_X = (d_{1,X}, d_{2,X}, d_{3,X})$  are displacements from the nucleotide centre-of-mass to interaction sites  $X$  in the local nucleotide frame; these are model-specific parameters controlling relative placement of interaction sites. The values of  $\mathbf{d}_X$  are as follows:

$$\mathbf{d}_{\text{back}}^1 = [-0.4, 0.0, 0.0] \quad (32)$$

$$\mathbf{d}_{\text{back}}^2 = [-0.34, 0.3408, 0.0] \quad (33)$$

$$\mathbf{d}_{\text{stack}} = [0.34, 0.0, 0.0] \quad (34)$$

$$\mathbf{d}_{\text{hb}} = [0.4, 0.0, 0.0] \quad (35)$$

$$(36)$$

where  $\mathbf{d}_{\text{back}}^1$  and  $\mathbf{d}_{\text{back}}^2$  are the displacement vectors for the backbone site in oxDNA1 and oxDNA2, respectively. In oxDNA2 (and oxRNA), several additional “ghost” sites are used in energy subterms (e.g. stacking) that do not have excluded volume; see Refs. [37] and [34] for details.

An oxDNA (or oxRNA) energy function is a function that maps a collection of center of masses  $\mathbf{R} \in \mathbb{R}^{n \times 3}$ , and orientations  $\mathbf{Q} \in \mathbb{R}^{n \times 4}$  to a scalar – it is the role of the energy function to determine the position of interaction sites. Thus, the parameters describing the relative position of the interaction sites can be thought of as parameters of the energy function that can be optimized via our method just as the parameters describing angular and radial terms. Our method could naturally be used to optimize these parameters though we present no such experiments in this work.

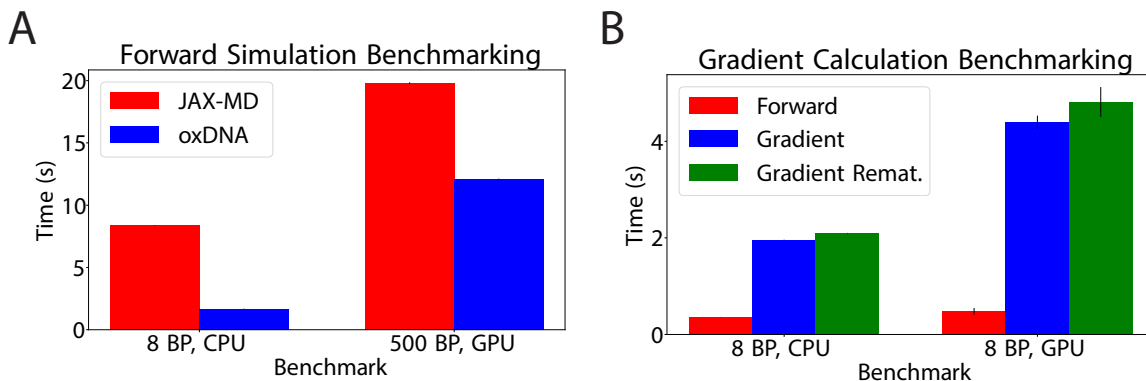


Figure S1: Benchmarking the overhead cost for **A.** forward simulations and **B.** gradient calculations in JAX-MD. In **A.**, a small system (8 base pair duplex) and large system (500 base pair duplex) were simulated for 50,000 timesteps using both the oxDNA standalone code and JAX-MD. The 8 base pair system was simulated on CPU without neighbor lists while the 500 base pair system was simulated on NVIDIA A100 GPU with Verlet lists. JAX-MD achieves comparable performance for the large system, taking 19.81 seconds vs. the 12.11 seconds with the standalone code. For short simulations of small systems, the overhead of JAX’s JIT-compilation exacerbates this difference. In **B.**, repeated the benchmarking from Figure 2D in the main text on both CPU and GPU, measuring the time to simulate the eight base pair system described above with and without gradient calculation. Gradient calculation through the unrolled trajectory imposes a significant time cost (0.36 s vs 1.96 s on CPU, 0.47 s vs 4.40 s on GPU). Gradient rematerialization enables gradient calculation through longer trajectories but at an additional time cost (1.96 s vs 2.10 s on CPU, 4.40 s vs 4.81 s on GPU). Observe that the small system runs faster on CPU.

## C Benchmarking

We first sought to benchmark performance for forward simulations via a pure JAX implementation of oxDNA vs. the standalone implementation. Our pure JAX implementation involves an implementation of the oxDNA energy function in JAX and relies on JAX-MD for integration and force calculation via automatic differentiation. We consider a small system (8 base pairs) and a large system (500 base pairs) on CPU and GPU, respectively; in Ref. [40], Sengar et al. highlight that small systems do not benefit from GPU acceleration. We also employ neighbor lists to accelerate the force calculation for the 500 base pair system. We observe a difference in runtime commensurate with the statistics reported by Schoenholz and Cubuk in their original presentation of JAX-MD [53]. For the large system, we observe a 64% increase in runtime. We observe a significantly larger runtime cost to simulate the small system in JAX-MD due to the fixed overhead of JIT-compilation.

We next sought to benchmark the overhead of gradient calculation via our JAX implementation. We considered only the 8 base pair system on both CPU and GPU. We also compared vanilla backpropagation through the unrolled trajectory with checkpointed gradients (every 100 timesteps), a method which can enable gradient calculation through longer simulations by reducing memory at the cost of runtime. For this system, vanilla backpropagation imposes a significant runtime overhead compared to forward simulations (approximately 450% and 850% on CPU and GPU, respectively). Gradient checkpointing imposes an additional 7-9% runtime increase. Note that this cost may be larger for longer time scales or more complex systems, but this is impossible to evaluate empirically as gradients cannot be computed for such simulations without checkpointing.



## D Optimizing Structural Properties

In this section, we describe the details of our structural optimization including simulation protocols and definitions of observables.

### D.1 Pitch

#### D.1.1 Definition

The *pitch* of a double-stranded DNA (or RNA) duplex describes the height of one complete helix turn, measured parallel to the helical axis; this is typically reported as the number of base pairs per helical turn. Consider a duplex comprised of two single strands,  $\alpha$  and  $\beta$ , each with  $n$  nucleotides. This duplex contains  $n$  base pairs where the  $i^{\text{th}}$  base pair involves the pairing of the  $i^{\text{th}}$  nucleotide of  $\alpha$  and the  $(n - i)^{\text{th}}$  nucleotide of  $\beta$ . For two adjacent base pairs  $i$  and  $j$ , we define the local helix axis as

$$\hat{\mathbf{h}} = \frac{\overline{\mathbf{h}\mathbf{b}_i} - \overline{\mathbf{h}\mathbf{b}_j}}{\|\overline{\mathbf{h}\mathbf{b}_i} - \overline{\mathbf{h}\mathbf{b}_j}\|} \quad (37)$$

where  $\overline{\mathbf{h}\mathbf{b}_i}$  denotes the mean hydrogen bonding site of the  $i^{\text{th}}$  base pair. We can then define  $\theta_{i,j}$ , the angle between the projections of two base-base vectors in a plane perpendicular to the helical axis, as

$$\theta_{i,j} = \arccos(\mathbf{back}_i^{\text{proj}} \cdot \mathbf{back}_j^{\text{proj}}), \quad (38)$$

where  $\mathbf{back}_i$  denotes the vector between the backbone sites in the  $i^{\text{th}}$  base pair and

$$\mathbf{back}_i^{\text{proj}} = \mathbf{back}_i - (\mathbf{back}_i \cdot \hat{\mathbf{h}}) \hat{\mathbf{h}} \quad (39)$$

Let  $O : \mathbb{R}^{2n \times 3} \rightarrow \mathbb{R}$  denote a map that computes the average angle  $\theta_{ij}$  for all adjacent base pairs,

$$O(\mathbf{R}) = \langle \theta_{i,i+1} \rangle_{i \in [n-1]} \quad (40)$$

In practice, the first two base pairs at each end of the duplex are not included in the calculation to remove the effects of fraying. We can then define the (differentiable) average  $\theta$  across many equilibrium states

$$\overline{\theta_{i,i+1}} = \mathbb{E}[O(\mathbf{R})]_{\mathbf{R} \sim \exp(-\beta U(\mathbf{R}))} \quad (41)$$

Finally, the expected pitch  $P$  is calculated as

$$P = \frac{2\pi}{\overline{\theta_{i,i+1}}} \text{ base pairs / turn} \quad (42)$$

Note that  $P$  is differentiable via the differentiability of  $\overline{\theta_{i,i+1}}$ . For pitch optimizations, we minimize the RMSE between Eq. 42 and a chosen target value.

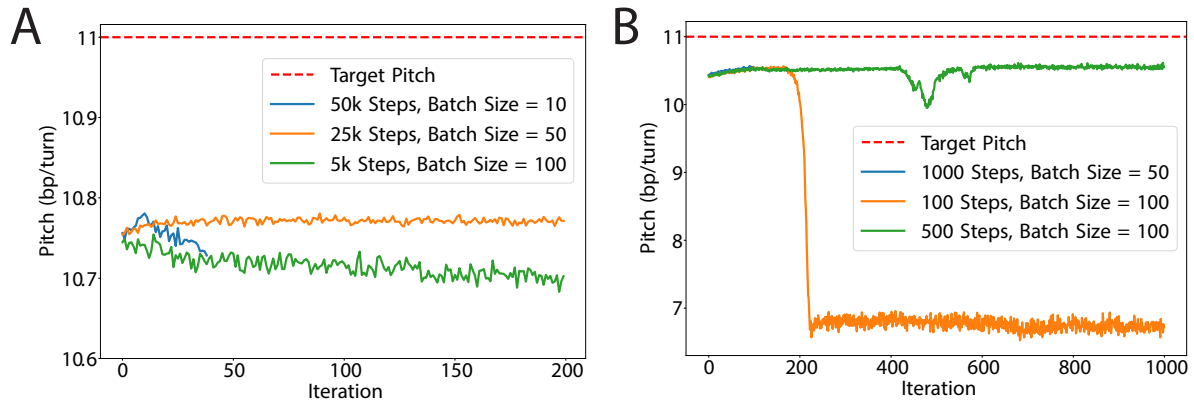


Figure S2: Benchmarking the performance of traditional stochastic gradient estimators for pitch optimization in oxDNA. Plots depict the pitch over time for optimizations using either the **A.** pathwise estimator or **B.** score function estimator, using a range of batch sizes and simulation lengths. Optimizations using the pathwise estimator and simulations of length 50,000 timesteps yielded nan values before the maximum number of iterations.

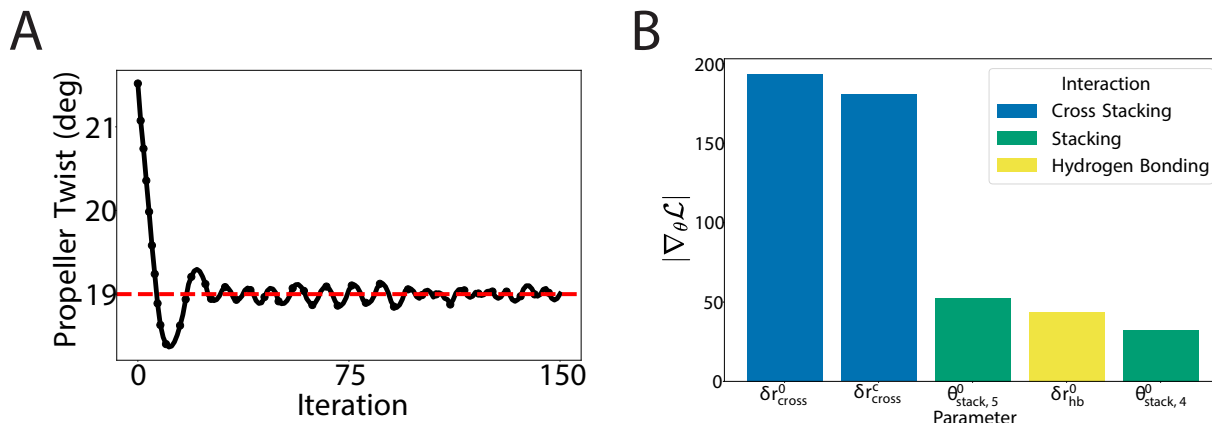


Figure S3: Optimization of oxDNA parameters for target propeller twist. **A.** The loss values over time, defined as the RMSE between the calculated propeller twist and a target propeller twist of  $19^\circ$ . **B.** The five most significant parameters ranked by the absolute value of their gradients.

### D.1.2 Optimization via Reparameterization Gradient

Despite the memory cost and numerical instabilities arising from differentiating through a simulation, we sought to evaluate the traditional pathwise estimator for pitch optimization. We defined the loss as the RMSE between the measured pitch and the target pitch. For a given simulation length and batch size (i.e. number of replicate simulations), we simulated a 60 base pair duplex using the Langevin integrator in JAX-MD and used the gradients computed via the pathwise estimator for gradient descent. Averages were computed from states sampled every 100 timesteps and all simulations were initialized with states obtained from 10,000 equilibration steps. All optimizations used a learning rate of 0.001. We found that the resultant gradient estimates did not yield optimized parameters for a range of simulation lengths and batch sizes (Figure S2A).

As structural properties are defined locally and therefore have particularly fast relaxation timescales, in practice we could mitigate these numerical instabilities by drastically increasing the friction coefficient, tantamount to decreasing the simulation time-step. However, this is not a tenable solution for many observables of interest as such an approach requires significantly longer simulations. We also note that numerical instabilities can be mitigated by gradient clipping but this method imposes its own numerical approximations and also requires significant time and memory overhead.

### D.1.3 Optimization via Score-Function Estimator

We then sought to evaluate the performance of the score function estimator). This requires obtaining a differentiable expression for the probability of each trajectory. The Langevin integrator in JAX-MD implements the integration scheme of Davidchak et al. [79] that follows a “BAOAB” splitting scheme [80], one choice for splitting the Langevin equation into deterministic and stochastic components. We represent the probability of a given timestep as the probability of the stochastic step in the integration scheme, and therefore the probability of a trajectory as the product of the probabilities over all timesteps. We extract this probability from JAX-MD and it is differentiable via JAX. All simulations were initialized with states obtained from 1,000 equilibration steps and all optimizations used a learning rate of 0.001.

Given a simulation length and batch size, we use this probability to obtain gradient estimates for pitch optimization for optimization. We evaluate a range of simulation lengths and batch sizes with a bias towards shorter simulations and higher batch sizes given the high variance introduced by longer simulations. In practice, we do not find any hyperparameter set that yields optimized parameter values. See Figure S2 for our results.

### D.1.4 Optimization via DiffTRE

The gradient estimator for the optimizations depicted in Figure 3 requires a set of reference states at each iteration. To sample reference states for a given set of parameters  $\hat{\theta}$ , we perform 10 parallel simulations of length 250,000 timesteps and sample states every 1,000 steps. The total number of reference states is therefore  $N_{\text{ref}} = 2,500$ . We resample reference states when (i)  $N_{\text{eff}} < \lambda N_{\text{ref}}$  with  $\lambda = 0.95$  or (ii) after five gradient updates. We sampled reference states

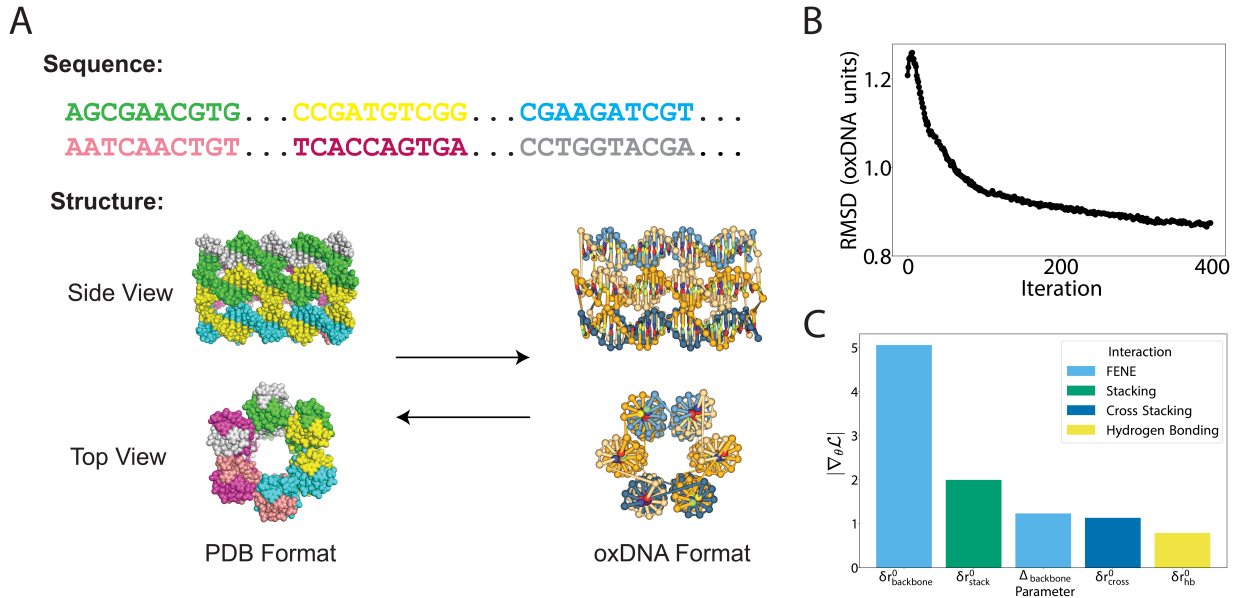


Figure S4: Fitting oxDNA parameters to a target sequence/structure. **A**. The gated DNA nanopore introduced in Ref. [61]. The structure is depicted both in PDB format and in the coarse-grained representation employed by oxDNA. **B**. The average RMSD of the simulated structure compared to the target structure throughout the optimization. **C**. Sensitivity analysis for the RMSD optimization, represented by the gradients with the top five largest absolute values from the first iteration.

using the standalone oxDNA code rather than JAX-MD, and automatically recompiled the executable for each updated parameter set. All optimizations used a learning rate of 0.001.

## D.2 Propeller Twist

In a DNA duplex, two paired bases do not typically align in the same plane. The *propeller twist* of a DNA duplex refers to the rotation of the base pairs around the axis perpendicular to the helical axis of the DNA.

Again, consider a duplex comprised of two single strands,  $\alpha$  and  $\beta$ , each with  $n$  nucleotides where the  $i^{\text{th}}$  base pair involves the pairing of the  $i^{\text{th}}$  nucleotide of  $\alpha$  and the  $(n - i)^{\text{th}}$  nucleotide of  $\beta$ . For the  $i^{\text{th}}$  base pair, let  $\mathbf{a}_{2,i}^{\alpha}$  and  $\mathbf{a}_{2,n-i}^{\beta}$  denote the vectors normal to the plane of the base for each of two base paired nucleotides (see Appendix B for the definition of  $\mathbf{a}_2$ ). The propeller twist of the  $i^{\text{th}}$  base pair is

$$\phi_i = \arccos(\mathbf{a}_{2,i}^{\alpha} \cdot \mathbf{a}_{2,n-i}^{\beta}) \quad (43)$$

The propeller twist of a single state for the is computed as the average twist over all base pairs,

$$O(\mathbf{R}) = \frac{1}{n} \sum_{i=1}^n \phi_i \quad (44)$$

As with pitch, the first two base pairs at each end are omitted due to fraying. The propeller twist  $T$  is understood to be the expected value computed across many equilibrium states,

$$T = \mathbb{E}[O(\mathbf{R})]_{\mathbf{R} \sim \exp(-\beta U(\mathbf{R}))} \quad (45)$$

## D.3 Sequence-Structure Pair

In machine learning, it is typical to train a model on known sequence-structure pairs (e.g. AlphaFold). We sought to demonstrate the flexibility of our method to accommodate such objective functions. As a simple example, we consider the gated DNA nanopore system of Burns et al. composed of six circular helices arranged in a ring [61].

We treated the unrelaxed structure deposited in Nanobase [60] as the ground truth, target structure (Figure S4). We used the negative simulated RMSD, measured via the oxDNA analysis tools [81], as a loss function. We successfully optimized the current oxDNA parameters to better match the unrelaxed structure as represented by a decrease in the average RMSD (Figure S4B). This example is relatively contrived as the unrelaxed structure contains unphysical bonds between adjacent helices and the optimization relaxes the parameters of the backbone FENE spring to accommodate this (see Figure S4C). Regardless, this serves as a simple demonstration of our ability to optimize directly for target sequence-structure pairs and to leverage off-the-shelf analysis tools, obviating the need for reimplementations. Each sampling of reference states involved 28 independent simulations of  $10^5$  timesteps with snapshots sampled every 1,000 steps.

## E Optimizing Mechanical Properties

### E.1 Persistence Length

Persistence length is a measure of stiffness, representing the length over which a polymer chain maintains a given direction before bending due to thermal fluctuations. We employ two methods for computing DNA persistence length: passively, by considering the decay in correlation length of tangent vectors; and simulating the force response of the DNA duplex and fitting to a worm-like chain (WLC) model. These approaches are described respectively below.

#### E.1.1 Passive calculation

For an infinitely long, semi-flexible polymer for which correlations in alignment decay exponentially with separation,  $L_{ps}$  obeys the following equality:

$$\langle \mathbf{l}_m \cdot \mathbf{l}_0 \rangle = \exp(-m\langle l_0 \rangle / L_{ps}) \quad (46)$$

where  $\mathbf{l}_0$  denotes the vector between the first two monomer and  $\langle \mathbf{l}_m \cdot \mathbf{l}_0 \rangle$  denotes the correlation between the first and  $n^{th}$  monomers [18, 65]. In practice,  $L_{ps}$  is computed by fitting the slope of the logarithm of this relationship, i.e.

$$\log(\langle \mathbf{l}_m \cdot \mathbf{l}_0 \rangle) = -m\langle l_0 \rangle / L_{ps} \quad (47)$$

Thus,  $L_{ps}$  can be calculated via simulation by sampling many equilibrium configurations, computing the average correlation of nucleotide tangent vectors as a function of separation, and extracting the persistence length according to Eq. 47.

We calculate the tangent vector to the  $i^{th}$  base pair,  $\mathbf{l}_i$ , to be the the (normalized) vector between the midpoints of that base pair and the adjacent base pair in the duplex:

$$\mathbf{l}_i = \frac{\mathbf{m}_{i+1} - \mathbf{m}_i}{\|\mathbf{m}_{i+1} - \mathbf{m}_i\|} \quad (48)$$

where  $\mathbf{m}_i$  denotes the midpoint of the base sites interacting in base pair  $i$ . For two base pairs  $i$  and  $j$  separated by  $m$  base pairs, the correlation between  $i$  and  $j$  can be expressed as

$$c_{ij} = \mathbf{l}_i \cdot \mathbf{l}_j \quad (49)$$

For a single snapshot of a duplex of length  $n$ , there are  $n - m$  such pairs of base pairs separated by  $m$  base pairs. Thus, the average correlation between base pairs separated by a distance  $m$  is

$$c_m = \frac{1}{n - m} \sum_{ij} c_{ij} \delta(j - i = m) \quad (50)$$

We compute an expected correlation for nucleotides separated by  $m$  base pairs over many snapshots, i.e.  $\mathbb{E}[O_m(\mathbf{R})]_{\mathbf{R} \sim \exp(-\beta U(\mathbf{R}))}$ . Given values for  $\mathbb{E}[O_m(\mathbf{R})]$  for  $1 \leq m \leq n$ , we can compute  $L_{ps}$  by fitting

$$\mathbb{E}[O_m(\mathbf{R})] = \exp(-m\langle l_0 \rangle / L_{ps}) \quad (51)$$

with  $\langle l_0 \rangle$  the average length of the tangent vectors, and extracting the slope,

$$L_{ps} = -\frac{\ln \mathbb{E}[O_m(\mathbf{R})]}{m\langle l_0 \rangle} \quad (52)$$

Crucially, the entire calculation of  $L_{ps}$  given a set of reference states can be made differentiable by combining DiffTRE and implicit differentiation.  $\mathbb{E}[O_m(\mathbf{R})]$  is differentiable for all  $m$  via reweighting and implicit differentiation can be used to differentiate the line-fitting procedure described in Equations 51 and 52 in the case where an analytic solution is not available.

Persistence length calculations notoriously require many uncorrelated states to obtain sufficient correlation statistics [18]. In all optimizations of  $L_{ps}$  via this passive calculation, we simulate a 60 bp duplex following Ref. [37]. Each calculation of  $L_{ps}$  involves 64 parallel simulations each comprising  $2.5 \times 10^6$  timesteps, sampling reference states every  $10^4$  steps. We neglect the first 2 base pairs on either end of the duplex due to boundary effects and only fit Equation 51 for  $m \leq 40$  as large  $m$  have poor statistics. We again use a learning rate of 0.001 and resample states via the same protocol as described for pitch optimizations.

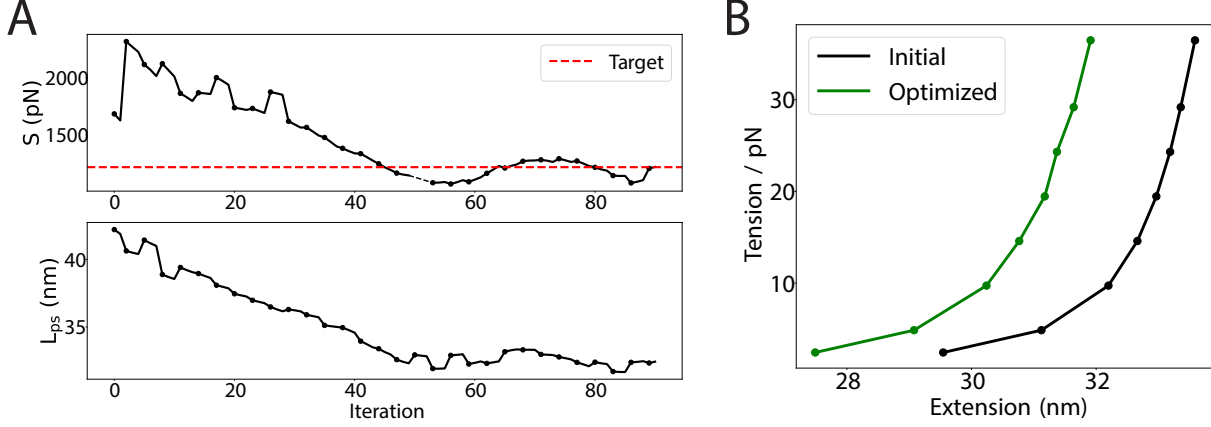


Figure S5: Optimization of stretch modulus via a worm-like chain fit in which the persistence length is constrained via a passive calculation. **A.** The stretch modulus and corresponding persistence length over time. **B.** The force extension curves corresponding to the initial and optimized parameters.

### E.1.2 Worm-like-chain (WLC) Fitting

Under low tension, a long molecule of dsDNA behaves like an extensible wormlike chain (WLC) [63]. Both persistence length  $L_{ps}$  and extensional modulus  $S$ , which quantifies the elastic resistance of dsDNA to stretching, can be extracted from fits to the WLC expression of Odjik *et al.*:

$$x = L_0 \left( 1 + \frac{F}{S} - \frac{k_B T}{2F} [1 + y \coth y] \right) \quad (53)$$

with

$$y = \left( \frac{F L_0^2}{L_{ps} k_B T} \right)^{1/2} \quad (54)$$

where  $x$  is the extension of the duplex under force  $F$ ;  $L_0$  is the contour length of the duplex; and  $k_B T$  is the thermal energy unit at temperature  $T$ .

In prior work [18, 57],  $S$  was calculated by applying tension to the middle 100 base pairs of a 100 base pair duplex and conducting an unconstrained three-parameter fit to Equation 53 to obtain  $S$ ,  $L_{ps}$ , and  $L_0$ . This process is amenable to gradient-based optimization by again combining DiffTRE and implicit differentiation. Consider a simulation of such a duplex under pulling force  $F_i$  that yields a collection of sampled states  $\vec{X}_i$ . Let  $O_i : \mathbb{R}^{3 \times n} \rightarrow \mathbb{R}$  be a function that computes the end-to-end distance of the 100 bp region subject to the pulling force  $F_i$ . The extension of the duplex is simply the arithmetic mean of extensions over all sampled states and therefore can be expressed as the following reweighted expectation:

$$\mathbb{E}[O_i(X)]_{X \sim \exp(-\beta U^{tot}(X))} = \sum_X w_X O_i(X) \quad (55)$$

with  $U^{tot}(X) = U^{ext}(X) + U(X)$  where  $U(X)$  denotes the Hamiltonian of the DNA model parameterized by  $\theta$  and  $U^{ext}(X)$  denotes the energetic contribution corresponding to the external force. This yields a set of weights

$$w_X = \frac{\exp\left(-\beta \left( U_{\theta}^{tot}(X) - U_{\hat{\theta}}^{tot}(X) \right)\right)}{\sum_{X'} \exp\left(-\beta \left( U_{\theta}^{tot}(X') - U_{\hat{\theta}}^{tot}(X') \right)\right)} \quad (56)$$

$$= \frac{\exp\left(-\beta \left( U_{\theta}^{ext}(X) + U_{\theta}(X) - U_{\hat{\theta}}^{ext}(X) - U_{\hat{\theta}}(X) \right)\right)}{\sum_{X'} \exp\left(-\beta \left( U_{\theta}^{ext}(X') + U_{\theta}(X') - U_{\hat{\theta}}^{ext}(X') - U_{\hat{\theta}}(X') \right)\right)} \quad (57)$$

$$= \frac{\exp\left(-\beta \left( U_{\theta}(X) - U_{\hat{\theta}}(X) \right)\right)}{\sum_{X'} \exp\left(-\beta \left( U_{\theta}(X') - U_{\hat{\theta}}(X') \right)\right)} \quad (58)$$

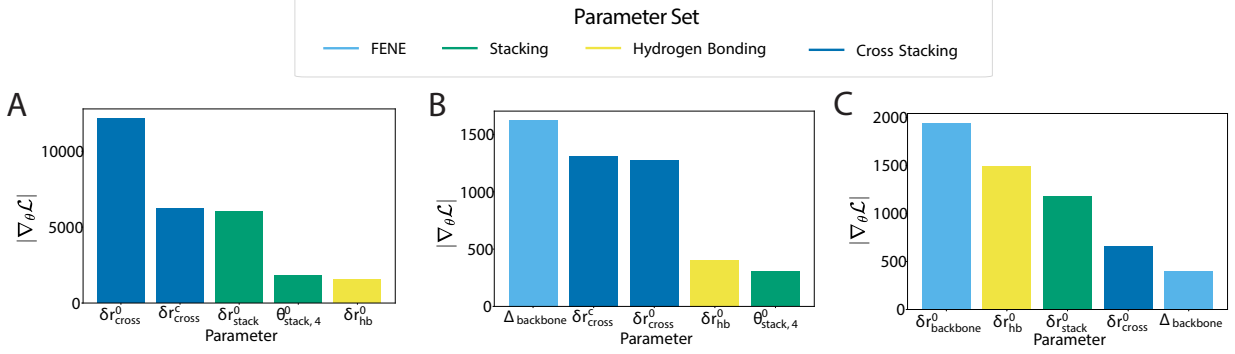


Figure S6: Sensitivity analysis for the stretch-torsion observables, represented by the five most significant parameters ranked by the absolute value of their gradients, for the **A.** effective stretch modulus  $S_{\text{eff}}$ , **B.** torsional modulus  $C$ , and **C.** twist-stretch coupling  $g$ .

Importantly, the contribution of  $U^{\text{ext}}$  to  $w_X$  cancels which is crucial to calculating  $w_X$  in practice as in general  $U^{\text{ext}}$  is not known for an arbitrary external force (or torque). This is also intuitive as  $U^{\text{ext}}$  has no *explicit* dependence on the parameters; i.e.  $\nabla_{\theta} U^{\text{ext}} = 0$ . With our differentiable estimate for the extension  $O_i$  under force  $F_i$  in hand, we can use nonlinear least squares to solve for  $S$  per Equation 53. As in the case of the passive persistence length calculation, we use implicit differentiation to differentiate this fitting procedure.

However, in practice, we find this calculation to be highly sensitive to small changes in parameter values which is an undesirable property for gradient-based optimization. To remedy this instability, we fix the persistence length via the passive calculation and compute  $S$  and  $L_0$  via the WLC fit. This yields stable optimization as shown in Figure S5.

We compute the persistence length with the parameters described above. For the WLC fit, we consider force values of 0.05, 0.1, 0.2, 0.3, 0.4, 0.5, 0.6, and 0.75 (in oxDNA units). The WLC fit requires a calculation of the extension under each force and therefore we perform a batch of simulations for each force. For each force, we perform 12 simulations of length  $2.5 \times 10^6$  timesteps and sample reference states every  $10^5$  steps. Low forces are particularly hard to resolve as there are larger fluctuations in conformational space, and we therefore simulate  $\times 4$  as many independent simulations for low forces (i.e. 0.05 and 0.1 oxDNA units). For comparison with Ref. [41], we perform this optimization using the oxDNA 1.0 force field. In total, sampling all reference states requires 232 independent simulations. We use Ray to distribute this calculation [82]. We use a learning rate of 0.001, and resample reference states with  $\lambda = 0.95$  or after three gradient updates.

To demonstrate the flexibility of our method, we also optimize only the sequence-specific parameters to achieve an arbitrarily chosen persistence length (Figure S8). Sequence specificity is implemented in recent versions of oxDNA via context-dependent scalars of the hydrogen bonding and stacking interactions, and equality between subsets of sequence-specific parameters is enforced to obey symmetries (e.g. 5' to 3' vs. 3' to 5'). We enforce all such symmetries in our optimization.

## E.2 Stretch and Torsional Moduli

An analogous quantity of interest is the *torsional modulus*  $C$ , which characterizes a polymer's resistance to twisting under external torque. Under the action of a non-zero external torque  $\tau$ , a DNA helix will twist some amount  $\Delta\theta$  beyond its equilibrium twist value  $\theta_0$  of  $\sim 35^\circ$  [83]:  $\Delta\theta = \theta - \theta_0$ , where  $\theta$  is the total twist. It can be shown that according to equipartition of energy, at zero torque, one can measure the fluctuations in  $\Delta\theta$  and extract the torsional modulus according to [84, 24]:

$$\langle \Delta\theta^2 \rangle = \frac{k_B T L_0}{C} \quad (59)$$

where  $\langle \Delta\theta^2 \rangle$  is the variance in deviation from equilibrium twist over some ensemble of samples and  $L_0$  is the equilibrium end-to-end extension of the DNA. In the original presentation of oxDNA,  $C$  was calculated using Monte Carlo moves chosen to enforce that the base pairs at the end of the central section remained perpendicular to the vector between their midpoints [18]. This allowed for an unambiguous definition of the axis about which torsion could be

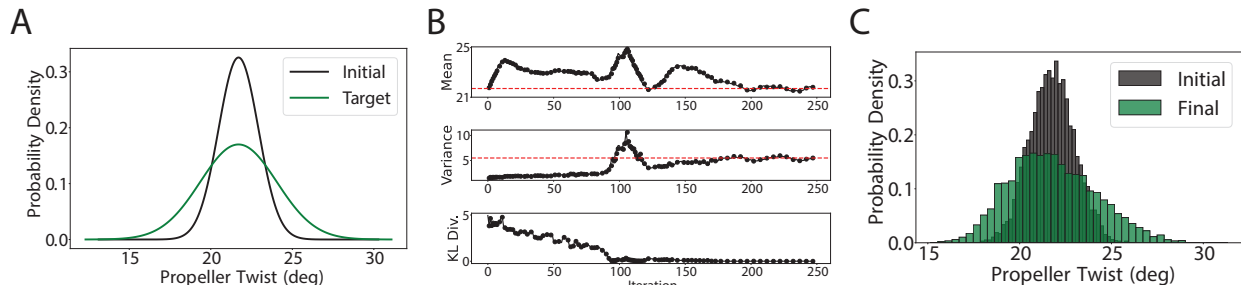


Figure S7: Fitting to a target propeller twist distribution. **A.** An overview of the optimization problem. The initial distribution of propeller twists is Gaussian with  $\mu = 21.7^\circ$  and  $\sigma^2 = 1.5$  and the objective is to minimize the KL-divergence with a target distribution. Here, we consider the case of increasing the variance ( $\sigma^2 = 5.5$ ) while maintaining the mean ( $\mu = 21.7^\circ$ ). **B.** The progression of the mean, variance, and KL-divergence (i.e. the loss) throughout the optimization. **C.** Histograms of the sampled propeller twists with the initial parameters and the optimized parameters.

applied and twist measured. However, such MC moves are not implemented in a publicly available software package and such constraints cannot be applied as rigorously in MD, yielding poor estimates of  $C$  using Eqn. 59.

We therefore follow the protocol of Assenza and Pérez [24] for calculating  $C$ . This involves subjecting a dsDNA duplex to various external forces and torques; measuring the changes in extension and twist due to external force and torque, respectively; and computing stretch modulus  $S$  and torsional modulus  $C$  via an analytic formula. This approach also allows for the extraction of the twist-stretch coupling constant  $g$ .

For a given force  $f$  and torque  $\tau$ , we simulate a 40 bp duplex subjected to the simultaneous action of a pulling force  $f$  and torque  $\tau$  along the  $z$ -axis. The molecule is initialized with its long axis along the  $z$ -axis and a harmonic constraint is applied to one end of the duplex to fix the position of two bottom base pairs. At the other end of the duplex, a pulling force with constant magnitude  $f$  is applied in the  $z$ -direction to the center of mass of the second base pair from the end and harmonic constraints are applied to  $x$ - and  $y$ -coordinates of the same base pair to maintain alignment with the  $z$ -axis. A constant torque  $\tau$  is applied to the two base pairs at the same end. See the section titled “Stretch–Torsion Simulations” in Ref. [24] for exact simulation details.

Following Ref. [24], we first performed simulations at  $\tau = 0$  for pulling forces  $f = 2, 4, 6, 8, 10, 15, 20, 25, 30, 35,$  and  $40$  pN. For each force  $f$ , we compute the extension  $\Delta L$  as

$$\langle \Delta L \rangle = \langle L \rangle - L_0 \quad (60)$$

where  $\langle L \rangle$  is average end-to-end extension over the set of reference states from the simulation under force  $f$  and  $L_0$  is the average extension under  $f = 0$  and  $\tau = 0$ . We then fit the linear dependence of  $\Delta L$  on the pulling force  $f$  at  $\tau = 0$  to extract the slope  $A_1$ ,

$$\langle \Delta L \rangle = A_1 f \quad (61)$$

Next, we then performed simulations at  $f = 2$  pN for values of the torque  $\tau = 0, 5, 10, 15, 20, 25,$  and  $30$  pN  $\cdot$  nm. For each simulation, we compute both  $\langle \Delta L \rangle$  (as defined above) and  $\langle \Delta \theta \rangle$  where

$$\langle \Delta \theta \rangle = \langle \theta \rangle - \theta_0 \quad (62)$$

where  $\langle \theta \rangle$  is the expected value of twist over the set of reference states from the simulation under torque  $\tau$  and  $\theta_0$  is the equilibrium twist under  $f = 0$  and  $\tau = 0$ . See Ref. [24] for a formal definition of  $L$  and  $\theta$ . We then fit the linear dependence of both the extension and the torsion angle on torque, extracting the slopes  $A_3$  and  $A_4$ , respectively ( $A_2$  is omitted for notational consistency with Ref [24]):

$$\langle \Delta L \rangle = \text{constant} + A_3 \tau \quad (63)$$

$$\langle \Delta \theta \rangle = \text{constant} + A_4 \tau \quad (64)$$



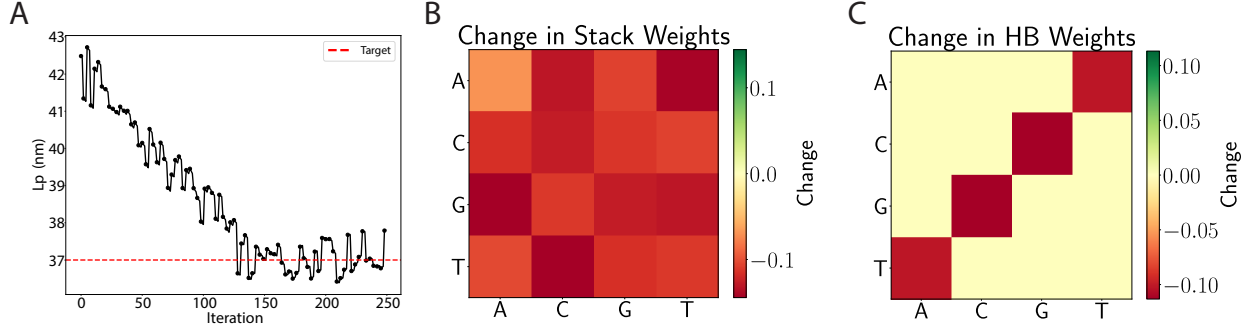


Figure S8: Fitting the sequence-specific stacking and hydrogen-bonding parameters to a target persistence length. **A.** The persistence length over time. **B-C.** The absolute change in the sequence-specific stacking and hydrogen bonding parameters between the initial and optimized values. We obey the same symmetries for sequence-specific parameters as described in Ref. [34]

Finally, we can compute  $C$ ,  $\tilde{S}$ , and  $g$  from  $A_1$ ,  $A_3$ , and  $A_4$  following the derivation given in Ref [24]:

$$\tilde{S} = \frac{L_0}{A_1} \quad (65)$$

$$C = \frac{A_1 L_0}{A_4 A_1 - A_3^2} \quad (66)$$

$$g = -\frac{A_3 L_0}{A_4 A_1 - A_3^2} \quad (67)$$

where  $\tilde{S} \equiv S - g^2/C$  is the effective extensional modulus. As in the case of the WLC fit and the passive calculation of  $L_{ps}$ , this entire calculation is made differentiable by reweighting the expectations computed in Equations 60 and 62 and using implicit derivatives for the line fitting procedures in Equations 63 and 64. In practice, a linear line fitting procedure has an analytical derivative.

Following Ref. [24], we use LAMMPS to sample reference states for each force-torque pair (see Ref. [24] for simulation parameters). For each force-torque pair, we perform three identical simulations of length  $2.5 \times 10^6$  timesteps and sample reference states every 2,500 steps. Before sampling reference states, we initiate each simulation with an equilibration period of 50,000 timesteps. We resample reference states with  $\lambda = 0.95$  or after five gradient updates.

In Figure 4 we also consider the experimental uncertainties of the torsional modulus, effective stretch modulus, and twist-stretch coupling. Consider an observable  $X$  with target value  $X^{target}$  and experimental uncertainty  $\epsilon_X$ . To account for this in our objective function, we use the following form:

$$\mathcal{L}(X^{sim}) = \begin{cases} 0 & \text{if } X_{lo}^{target} \leq X^{sim} \leq X_{hi}^{target} \\ \text{RMSE}(X^{sim}, X_{lo}^{target}) & \text{if } X^{sim} < X_{lo}^{target} \\ \text{RMSE}(X^{sim}, X_{hi}^{target}) & \text{otherwise} \end{cases} \quad (68)$$

where  $X_{lo}^{target} = X^{target} - \epsilon_X$ ,  $X_{hi}^{target} = X^{target} + \epsilon_X$ , and  $X^{sim}$  is the value of  $X$  measured via simulation.

## F Thermodynamic Optimization

In this section, we describe the details of our thermodynamic optimization including enhanced sampling protocols, simulation details, temperature extrapolation, finite size corrections, line fitting procedures, and observable definitions.

### F.1 Duplex Melting Temperature Calculation

The melting temperature ( $T_m$ ) of a DNA duplex is defined as the temperature at which 50% of the DNA strands are bound in a duplex and 50% of the DNA strands remain unbound as single-stranded DNA. In general, binding and unbinding events occur on long timescales and therefore require enhanced sampling methods to calculate via simulation.

At a high level, melting temperature calculations are performed in oxDNA as follows. Given a DNA duplex, a discrete order parameter is assigned to each base pair indicating whether or not the two nucleotides are bound. Thus, a global order parameter indicating the total number of base pairs for a given state can be defined; a state is defined as bound if it has at least one base pair and unbound otherwise. Next, a biased simulation is run at a single temperature in which an umbrella weight is assigned to each possible number of base pairs. The simulation results are then unbiased to obtain the number of states visited in the bound and unbound states. These counts are then extrapolated to a range of temperatures and a finite size correction is applied to the extrapolated counts. Finally, a melting curve is fit to the ratio of bound to unbound counts at each temperature and the melting temperature is determined as the temperature at which there are 50% bound and 50% unbound states.

Formally, consider a system of two complimentary sequences of single-stranded DNA of length  $n$  that can base pair to form a duplex. The  $i^{th}$  base pair is comprised of the  $i^{th}$  and the  $(2n - i + 1)^{th}$  nucleotides with the first and second strands represented by nucleotides indexed by  $[1, n]$  and  $[n + 1, 2n]$ , respectively. Given a configuration  $R \in \mathbb{R}^{2n \times 3}$ , assume the existence a base-pair level order parameter

$$B(i) = \begin{cases} 1 & \text{if } R_i \text{ and } R_{2n-i+1} \text{ are bonded} \\ 0 & \text{otherwise} \end{cases} \quad (69)$$

We can then define a state-level order parameter that computes the total number of base pairs,

$$N(R) = \sum_{i=1}^n B(i) \quad (70)$$

Since there are  $n$  possible base pairs,  $N(R) \in [0, n]$ . We then define a vector of umbrella weights  $\omega \in \mathbb{R}^{n+1}$  where  $\omega_i$  denotes the umbrella weight applied to a state with  $i$  base pairs. If  $U : \mathbb{R}^{2n \times 3} \rightarrow \mathbb{R}$  denotes the oxDNA energy function, umbrella sampling via these weights will sample states from the following probability distribution:

$$p(R) = \frac{\omega_{N(R)} \exp(-\beta U(R))}{Z} \quad (71)$$

where

$$Z = \int \omega_{N(R')} \exp(-\beta U(R')) dR' \quad (72)$$

Next, we sample a trajectory of  $T$  states  $\vec{R} \in \mathbb{R}^{T \times 2n \times 3}$  from this distribution via virtual-move Monte Carlo (VMMC) at temperature  $\tau$ . Given this trajectory, we can compute the biased number of states with  $i$  base pairs,  $S_i$ :

$$S_i^{biased} = \sum_{t=1}^T \delta(N(\vec{R}_t) = i) \quad (73)$$

For an arbitrary state-level observable  $A$ , the expected value with respect to a set of states sampled from an umbrella sampling simulation can be computed as

$$\langle A \rangle = \frac{\langle A/\omega \rangle_{\vec{R}}}{\langle 1/\omega \rangle_{\vec{R}}} \quad (74)$$

where  $\omega$  denotes the umbrella weight for a given state. Thus, we can obtain an unbiased value of  $S_i$ ,

$$S_i^{unbiased} = \sum_{t=1}^T \frac{1}{\omega_i} \delta(N(\vec{R}_t) = i) \quad (75)$$

where we ignore the normalization factor as we only care about ratios of counts when computing  $T_m$ . In the same manner, given a simulation at temperature  $\tau$ , one can treat this simulation as a biased sample of the ensemble at another temperature  $\tau'$  and the expected value of an observable  $A$  can be corrected in the same way as in umbrella sampling [40]:

$$\langle A(x) \rangle_{\tau'} = \langle A(x) \exp(U(x, \tau)/k\tau - U(x, \tau')/k\tau') \rangle \quad (76)$$

Note that in oxDNA  $U(x, \tau')$  is different than  $U(x, \tau)$  due to the temperature-dependence of the stacking term in the interaction energy. Thus, given our set of states sampled at temperature  $\tau$  with our umbrella weights  $\vec{\omega}$ , we can obtain an unbiased value of  $S_i$  at temperature  $\tau'$ :

$$S_{i, \tau'}^{unbiased} = \sum_{t=1}^T \frac{1}{\omega_i} \exp(\Delta U(\vec{R}_t)_{\tau'}) \delta(N(\vec{R}_t) = i) \quad (77)$$

where

$$\Delta U(\vec{R}_t)_{\tau'} = U(\vec{R}_t, \tau)/k\tau - U(\vec{R}_t, \tau')/k\tau' \quad (78)$$

Again, we omit the normalizing factor. Given  $S_{i, \tau'}^{unbiased}$  for  $i \in [0, n]$  for a given temperature  $\tau'$ , we then compute the total number of bound and unbound states as

$$S_{\text{bound}, \tau'} = \sum_{i=1}^n S_{i, \tau'}^{unbiased} \quad (79)$$

$$S_{\text{unbound}, \tau'} = S_{0, \tau'}^{unbiased} \quad (80)$$

and define the relative probability with which bound and unbound states are observed as

$$\Phi_{\tau'} = \frac{S_{\text{bound}, \tau'}}{S_{\text{unbound}, \tau'}} \quad (81)$$

The fraction of bound pairs can then be expressed as

$$f_{1, \tau'} = \frac{\Phi}{1 + \Phi} \quad (82)$$

Importantly,  $f_{1, \tau'}$  is computed using states sampled from a simulation of two DNA strands in a finite-sized box with periodic boundaries. In practice, this quantity is affected by fluctuations in the local concentration of reactants and therefore  $f_{1, \tau'} \neq f_{\infty, \tau'}$  where  $f_{\infty, \tau'}$  is the bulk equilibrium bonding fraction at the same temperature and concentration. To account for this source of error, we apply the correction introduced by Ouldridge [57]:

$$f_{\infty, \tau'} = \left(1 + \frac{1}{2\Phi}\right) - \sqrt{\left(1 + \frac{1}{2\Phi}\right)^2 - 1} \quad (83)$$

For a set of evenly-spaced temperatures  $\{\tau_{l_0}, \dots, \tau_{h_i}\}$ , we apply Equations 77-83 to compute  $\{f_{\infty, \tau_{l_0}}, \dots, f_{\infty, \tau_{h_i}}\}$ . Finally, we interpolate to find the temperature  $\tau^*$  at which  $f_{\infty, \tau^*} = 0.5$ . We can similarly interpolate to compute the width of the melting curve where

$$T_{\text{width}} = \tau_{0.2} - \tau_{0.8} \quad (84)$$

where  $\tau_{0.2}$  and  $\tau_{0.8}$  are the temperatures at which the bulk equilibrium bonding fraction is 0.2 and 0.8, respectively.

Given a set of reference states sampled at a single temperature  $\tau$  subject to umbrella weights  $\omega$ , the calculation of the melting temperature (and melting curve width) are differentiable via trajectory reweighting and implicit differentiation. Consider the calculation of  $S_{i, \tau'}^{unbiased}$  via Equation 77. As this quantity is a sum rather than an expected value and therefore the contribution of each state is scaled by 1 rather than  $1/N$  in the case where  $\theta = \hat{\theta}$ , we rewrite Equation 77 as

$$S_{i, \tau'}^{unbiased} = \sum_{t=1}^T \frac{T}{w_i} \frac{1}{\omega_i} \exp(\Delta U(\vec{R}_t)_{\tau'}) \delta(N(\vec{R}_t) = i) \quad (85)$$

where  $w_i$  is the DiffTRE weight for the  $i^{\text{th}}$  state. Importantly,  $\frac{N}{w_i} = 1$  when  $\theta = \hat{\theta}$ . Additionally, as  $\nabla_{\theta}\omega = 0$ , such prefactors can be computed. However, given the temperature dependent stacking term in the oxDNA potential,  $\nabla_{\theta} \exp(\Delta U(\vec{R}_t)_{\tau'}) \neq 0$  in the general case where  $\theta$  includes stacking parameters. The oxDNA standalone code

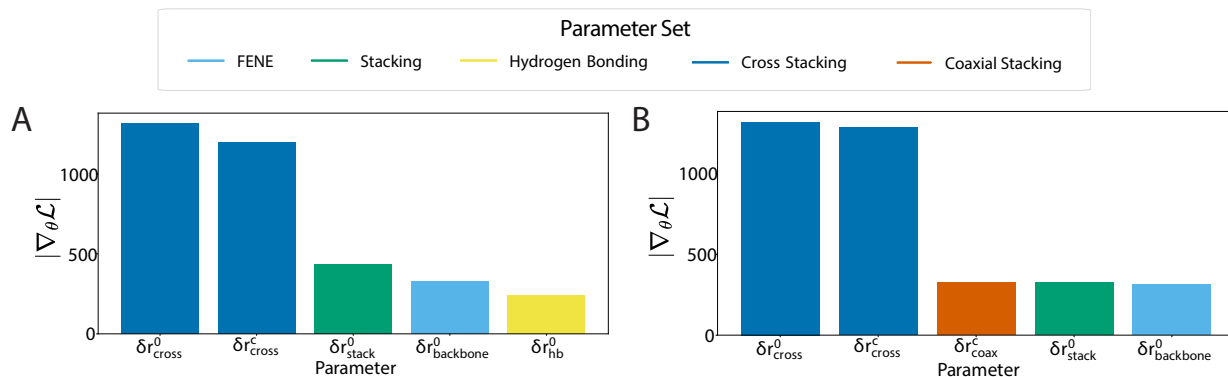


Figure S9: Sensitivity analysis for the **A.** duplex and **B.** hairpin  $T_m$  optimizations, represented by the five most significant parameters ranked by the absolute value of their gradients.

uses an energy threshold for computing  $B(i)$  and therefore  $\nabla_{\theta} B(i) \neq 0$  but as this quantity is thresholded (and not continuous) we neglect this term; we find that this is a reasonable approximation in practice. Given our differentiable formulation of  $S_{i, \tau'}^{\text{unbiased}}$  in Equation 85, the remaining calculation of the melting temperature and width require elementary differentiable operators, including the process of one-dimensional linear interpolation.

Above, we describe our method of differentiable melting curve calculation via a single order parameter (i.e. number of base pairs). In practice, we use a second order parameter, the inter-strand center of mass distance, to accelerate sampling. Equation 85 can flexibly accommodate an arbitrary number of order parameters as the delta function can be evaluated for an arbitrary subset of order parameters while the weight for a given state  $\omega_i$  depends on all biased order parameters used in sampling.

Computing  $T_m$  values requires sampling many uncorrelated states. To sample reference states, we perform 34 individual simulations of  $5 \times 10^7$  virtual-move Monte Carlo (VMMC) steps, sampling snapshots every  $2.5 \times 10^5$  steps. We perform biased simulations at 307.15 K. We resample reference states with  $\lambda = 0.95$  or after three gradient updates. All duplex  $T_m$  calculations are done with the oxDNA 1.0 force field rather than oxDNA 2.0.

## F.2 Hairpin Melting Temperature Calculation

The (differentiable) calculation of hairpin melting temperatures and melting curve widths is nearly identical to that of duplexes. However, since hairpin melting is the behavior of a single strand rather than of two independent strands, the melting behavior is not affected by fluctuations in the local concentration of single strands. Therefore,  $f_{1, \tau'} \neq f_{\infty, \tau'}$  and Equation 83 is not applied. As in the case of duplex melting, we use two order parameters for umbrella sampling – (1) the number of base pairs and (2) the binned minimum distance between all complementary nucleotides. We referenced <https://github.com/WillTKaufhold1/oxdna-tutorial> for an example implementation of such a simulation.

As with duplex  $T_m$ 's, accurately computing hairpin  $T_m$ 's requires sampling many uncorrelated states. To sample reference states, we perform 32 independent simulations of  $2.5 \times 10^7$  VMMC steps, sampling snapshots every 50,000 steps. We perform biased simulations at 330.15 K. Reference states are resampled via the same criteria as with duplex  $T_m$ 's.